

In the format provided by the authors and unedited.

Optogenetic control of gene expression in plants in the presence of ambient white light

Rocio Ochoa-Fernandez ^{1,2}, Nikolaj B. Abel ³, Franz-Georg Wieland ⁴, Jenia Schlegel^{2,5}, Leonie-Alexa Koch¹, J. Benjamin Miller ⁶, Raphael Engesser⁴, Giovanni Giuriani^{1,7}, Simon M. Brandl³, Jens Timmer^{4,8}, Wilfried Weber ^{3,8}, Thomas Ott ^{3,8}, Rüdiger Simon ^{2,5,9} and Matias D. Zurbriggen ^{1,2,9} 

¹Institute of Synthetic Biology, University of Düsseldorf, Düsseldorf, Germany. ²iGRAD Plant Graduate School, University of Düsseldorf, Düsseldorf, Germany. ³Faculty of Biology, University of Freiburg, Freiburg im Breisgau, Germany. ⁴Institute of Physics, University of Freiburg, Freiburg im Breisgau, Germany. ⁵Institute of Developmental Genetics, University of Düsseldorf, Düsseldorf, Germany. ⁶School of Biological Sciences, University of East Anglia, Norwich, UK. ⁷University of Glasgow, Glasgow, Scotland, UK. ⁸Signalling Research Centres BLOSS and CIBSS, University of Freiburg, Freiburg im Breisgau, Germany. ⁹CEPLAS—Cluster of Excellence on Plant Sciences, Düsseldorf, Germany. e-mail: matias.zurbriggen@uni-duesseldorf.de

Supplementary Note. Development and calibration of the mathematical model

1. Describing PULSE with a mathematical model

We developed a mathematical model to describe the complex dynamical changes of the optogenetic PULSE system systematically. The modelling is performed by creating a model of the system using kinetic rate equations. These equations describe the dynamics underlying the entire system with ten dynamic parameters.

Experimental limitations make it impossible to measure all concentrations at play. Only the FLuc protein levels as well as FLuc-mRNA levels can be measured. Thus, by only inferring parameters from single experiments, the processes underlying the optogenetic activation and repression cannot be described reliably. For this reason, we used a comprehensive approach, in which all experiments are used as joint basis to infer parameters from the model. Using this approach makes it possible to infer all parameters and their uncertainties. This methodology has been widely used and is the standard in the field¹⁻⁴.

In order to use this approach, the experimental data under different conditions have to be made comparable, thus a scaling parameter is included for each experimental dataset. We estimated these scaling parameters together with dynamical parameters and the initial concentration of FLuc.

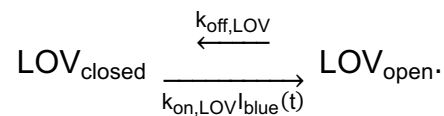
Including the error estimation, this leads to 24 parameters, which were inferred simultaneously from all experimental data, making it possible to describe the optoswitch with reliably determined parameters.

In the following, we describe the modelling process in detail. In Section 2, we derive the mathematical model with its equations, while Section 3, introduces the methodology of the parametrization and uncertainty analysis of the model. Furthermore, Section 4 characterizes the link to the experimental data and Sections 5 and 6 show the results of the parameter estimation and the predictions of the model.

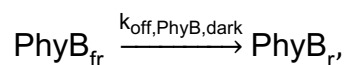
2. Derivation of the mathematical model

We derive a mathematical model for PULSE in the following chapter based on ordinary differential equations.

The EL222 photoreceptor consists of the LOV-J α -HTH domains (LOV) and has a light-dependent transitioning behaviour between its two conformations. It transitions to its folded state LOV_{closed} with a constant rate $k_{\text{off,LOV}}$ and unfolds into its active open state LOV_{open} under blue light (460 nm) with the rate $k_{\text{on,LOV}} I_{\text{blue}}(t)$, dependent on the light intensity

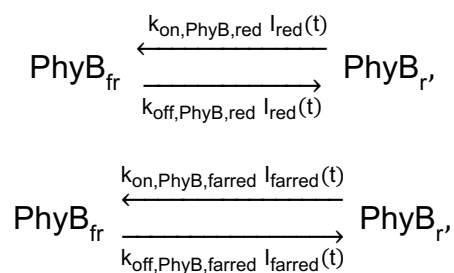


The interaction factor PhyB-VP16 is similarly light-dependent. The light-sensitive Phytochrome B (PhyB) has two conformational states, an active state sensitive to far-red light PhyB_{fr} in which it can bind to PIF6 as well as an inactive state sensitive to red light PhyB_r. A constant revision from the active to the inactive state is modelled



therefore, in the dark all of the complex will be in its inactive state.

Under both far-red light (740 nm) in the infrared spectrum as well as red light (660 nm) the two conformations exhibit probabilistic conformational changes into each other



dependent on the light intensities $I_{\text{farred}}(t)$ and $I_{\text{red}}(t)$.

The reporter Firefly luciferase (FLuc) mRNA is transcribed with a basal production $b_{\text{transcription}}$ and degraded with a constant degradation rate $k_{\text{deg,FLuc mRNA}}$. Furthermore, the activation of the mRNA transcription by the active state of the PhyB-VP16 complex PhyB_{fr} is modelled by the Michaelis-Menten reaction with the rate $k_{\text{transcript,extended}}$ and the Michaelis-Menten constant K_m . However, the activated EL222 (LOV_{open}) inhibits this activation. The Michaelis-Menten constant $K_{m_inhibition}$ of this process is inverse to the strength of the inhibition. $k_{\text{inh,LOV}} = K_{m_inhibition}^{-1}$ is used in the modelling of the process. It has the unit of $[1/\mu\text{M}]$. To account for cooperative binding effects a Hill-coefficient of two is used for the inhibition. Thus, the total dynamic transcription including the two non-competitive inhibitions becomes

$$\frac{d[\text{FLuc}_{\text{mRNA}}](t)}{dt} = \frac{k_{\text{transcript,extended}} [\text{PhyB}_{\text{fr}}]}{(K_m + [\text{PhyB}_{\text{fr}}]) (1 + k_{\text{inh,LOV}}^2 [\text{LOV}_{\text{open}}]^2)}$$

The extended model including this reactions shows two linearly dependent parameters $k_{\text{transcript,extended}}$, and K_m . Both parameters are non-identifiable and compatible with infinity (**Supplementary Fig. 8**). Their ratio, however, is constant and thus can be used to create an identifiable parameter

$$\frac{k_{\text{transcript,extended}}}{K_m} = k_{\text{transcript}} = \text{const.}$$

Using this ratio and setting K_m to infinity

$$\lim_{K_m \rightarrow \infty} \frac{k_{\text{transcript,extended}} [\text{PhyB}_{\text{fr}}]}{(K_m + [\text{PhyB}_{\text{fr}}]) (\blacksquare)} = \lim_{K_m \rightarrow \infty} \frac{k_{\text{transcript}} [\text{PhyB}_{\text{fr}}]}{(1 + \frac{[\text{PhyB}_{\text{fr}}]}{K_m}) (\blacksquare)} = \frac{k_{\text{transcript}} [\text{PhyB}_{\text{fr}}]}{(\blacksquare)},$$

where \blacksquare describes the inhibition term due to the LOV system, leads to a simplification of the transcription. This simplification can be explained by the fact, that the Michaelis-Menten reaction is in its linear limit, *i.e.* the saturation does not influence the behaviour of the system for the measured conditions. The full equation describing the transcription thus becomes

$$\frac{d[\text{FLuc}_{\text{mRNA}}](t)}{dt} = \frac{k_{\text{transcript}} [\text{PhyB}_{\text{fr}}]}{1 + k_{\text{inh,LOV}}^2 [\text{LOV}_{\text{open}}]^2}$$

The target protein FLuc is translated from the $\text{FLuc}_{\text{mRNA}}$ with the rate $k_{\text{transl,FLuc}}$. It degrades linearly with the rate $k_{\text{deg,FLuc}}$.

This leads us to the full set of coupled differential equations describing the model:

blue light sensitive, closed LOV complex

$$\frac{d[\text{LOV}_{\text{closed}}](t)}{dt} = k_{\text{off,LOV}} [\text{LOV}_{\text{open}}] - k_{\text{on,LOV}} I_{\text{blue}}(t) [\text{LOV}_{\text{closed}}] \quad (1)$$

open LOV complex

$$\frac{d[\text{LOV}_{\text{open}}](t)}{dt} = -k_{\text{off,LOV}} [\text{LOV}_{\text{open}}] + k_{\text{on,LOV}} I_{\text{blue}}(t) [\text{LOV}_{\text{closed}}] \quad (2)$$

active PhyB complex, sensitive to red and far-red light with different rates

$$\begin{aligned} \frac{d[\text{PhyB}_{\text{fr}}](t)}{dt} = & k_{\text{on,PhyB,red}} I_{\text{red}}(t) [\text{PhyB}_{\text{r}}] - k_{\text{off,PhyB,red}} I_{\text{red}}(t) [\text{PhyB}_{\text{fr}}] \\ & + k_{\text{on,PhyB,farred}} I_{\text{farred}}(t) [\text{PhyB}_{\text{r}}] - k_{\text{off,PhyB,farred}} I_{\text{farred}}(t) [\text{PhyB}_{\text{fr}}] \\ & - k_{\text{off,PhyB,dark}} [\text{PhyB}_{\text{fr}}] \end{aligned} \quad (3)$$

inactive PhyB complex, sensitive to red and far-red light with different rates

$$\begin{aligned} \frac{d[\text{PhyB}_{\text{r}}](t)}{dt} = & -k_{\text{on,PhyB,red}} I_{\text{red}}(t) [\text{PhyB}_{\text{r}}] + k_{\text{off,PhyB,red}} I_{\text{red}}(t) [\text{PhyB}_{\text{fr}}] \\ & - k_{\text{on,PhyB,farred}} I_{\text{farred}}(t) [\text{PhyB}_{\text{r}}] + k_{\text{off,PhyB,farred}} I_{\text{farred}}(t) [\text{PhyB}_{\text{fr}}] \\ & + k_{\text{off,PhyB,dark}} [\text{PhyB}_{\text{fr}}] \end{aligned} \quad (4)$$

mRNA of FLuc including basal transcription and degradation

$$\begin{aligned} \frac{d[\text{FLuc}_{\text{mRNA}}](t)}{dt} = & b_{\text{transcription}} - k_{\text{deg,FLuc}_{\text{mRNA}}} [\text{FLuc}_{\text{mRNA}}] \\ & + \frac{k_{\text{transcript}} [\text{PhyB}_{\text{fr}}]}{1 + k_{\text{inh,LOV}}^2 [\text{LOV}_{\text{open}}]^2} \end{aligned} \quad (5)$$

FLuc protein including basal degradation

$$\frac{d[\text{FLuc}](t)}{dt} = k_{\text{transl,FLuc}} [\text{FLuc}_{\text{mRNA}}] - k_{\text{deg,FLuc}} [\text{FLuc}] \quad (6)$$

3. Parametrization of the model and identifiability analysis with maximum likelihood approach

We used a maximum likelihood approach to determine the unknown parameters of the model by fitting it to the experimental data. The identifiability analysis was performed using the profile likelihood method. Both methods were previously described in the supporting information of Beyer *et al.*⁵ and the following introduction is based on this description.

The ordinary differential equations (1)-(6) describing the model can be generalized to

$$\frac{d}{dt} \vec{x}(t) = \vec{f}(\vec{x}, \vec{p}, \vec{u}(t)) \quad (7)$$

where \vec{x} is the state vector of the system describing the dynamics of the concentrations and \vec{p} contains the dynamic parameters. $\vec{u}(t)$ is a function containing the external inputs. The initial conditions of the concentrations, *i.e.* the concentrations at the time $t = 0$ are given by $\vec{x}(0) = \vec{x}_0$. Since the concentrations themselves can not be measured, an observation function

$$y(t) = g(\vec{x}(t), \vec{s}) + \vec{\varepsilon}(t) \quad (8)$$

is necessary for each experiment to link the measured data to the model states $\vec{x}(t)$. The observation parameters \vec{s} contain the scaling parameters of the measurements.

We used a constant Gaussian error model with variance σ^2 to model the measurement error, *i.e.*

$$\varepsilon(t) \sim N(0, \sigma^2). \quad (9)$$

Using this error model, the probability of the measured data from \vec{y}^D from a single experiment with N_D data points given the complete set of parameters $\vec{\theta} = (\vec{p}, \vec{x}_0, \vec{s}, \sigma)$ becomes

$$L(\vec{y}^D, \vec{\theta}) = \prod_{j=1}^{N_D} \exp\left(-\frac{(y_j^D - g(\vec{x}(t_j), \vec{s}))^2}{2\sigma^2}\right). \quad (10)$$

Here $\vec{x}(t_j)$ denotes the concentrations at the time of the measurement y_j^D . Combining N_{exp} experiments leads to the likelihood function

$$L(\vec{y}^D, \vec{\theta}) = \prod_{k=1}^{N_{exp}} L(\vec{y}^{D_k}, \vec{\theta}_k). \quad (11)$$

The parameters, for which the data is most probable, *i.e.* the parameter set with the maximum likelihood can be found with the maximum likelihood estimator

$$\hat{\theta} = \underset{\vec{\theta}}{\operatorname{argmax}} (L(\vec{y}^D, \vec{\theta})). \quad (12)$$

For numerical reasons, it is more efficient to minimize the equivalent

$$\begin{aligned} -2\log L &= \sum_{j=1}^{N_D} \exp\left(-\frac{(y_j^D - g(\vec{x}(t_j), \vec{s}))^2}{2\sigma^2}\right) + 2 N_D \log(\sqrt{2\pi} \sigma^2) \\ &= \chi^2(\vec{\theta}) + 2 N_D \log(\sqrt{2\pi} \sigma^2) =: \chi_{mod}^2(\vec{\theta}). \end{aligned} \quad (13)$$

This term contains the sum of the weighted residuals $\chi^2(\vec{\theta})$ as well as an error model correction term.

We performed the uncertainty and identifiability analysis of the parameters using the profile likelihood method⁶. The profile likelihood of parameter θ_i is determined by

$$\chi_{PL}^2(\theta_i) = \min_{\theta_{i \neq j}}(\chi_{mod}^2(\vec{\theta})). \quad (14)$$

The 95 % confidence intervals of parameter θ_i can then be calculated by

$$CI(\theta_i) = \{ \theta \mid \chi_{PL}^2(\theta) - \chi_{PL}^2(\vec{\theta}) < \chi^2(95\%, df = 1) \}. \quad (15)$$

$\chi^2(95\%, df = 1)$ describes the 95th quantile of the χ^2 - distribution with one degree of freedom.

4. Implementation of the single experiments, simplifications of the model, and stoichiometric considerations

Each experiment used for the calibration of the model needs a specific observation function. We first normalized the observed FLuc or FLuc mRNA concentrations over a constitutive control. Then we linked the normalized concentrations to the internal states of FLuc and FLuc mRNA with a scaling factor. Thus, only relative concentrations are considered.

In general, not all protoplasts are transformed and thus FLuc transcripts only derive from transfected protoplasts. In contrast, the constitutive control's transcripts derive from all protoplasts. Thus, the normalized concentrations contain an unknown factor scaling the normalized concentrations of FLuc and FLuc mRNA with the fraction of

transfected cells. In our modelling process, this scaling is entailed in the scaling parameter of each experiment and does not alter the model's description of the system and its predictions.

a. Experiment 1: Characterization of the system after 18 h of illumination

In the first experiment (shown in **Fig. 3c**) we measured the FLuc concentrations after 18 h of expression under different light conditions with six replicates per measurement. FLuc concentrations were normalized using RLuc as normalization factor. Results of four independent representative experiments were used for the parameterization, necessitating a scaling factor for each repetition. The observation function of the normalized FLuc of repetition i thus becomes

$$\frac{\text{FLuc_observed}}{\text{RLuc_observed}} = \text{scale}_{\text{FLuc,Exp1,Rep}_i} [\text{FLuc}]. \quad (16)$$

The constant Gaussian error parameter for the experiment is the same for all four repetitions.

b. Experiment 2: Characterization of the system kinetics

In the second experiment (shown in **Extended Data Fig. 1a**) we measured a time series of the FLuc concentrations with six different light regimes and three replicates per measurement. In brief, protoplasts transformed for PULSE-controlled FLuc expression were kept in darkness for 12 h. Illumination was started and after 3 h of red light-treatment, the samples were divided and incubated for the next 13 h: either i) in red light to quantify sustained activation, ii) transferred to darkness to assess the passive reversion of the system, or iii) transferred to blue light to determine active shut down of the system (On-Off). We observed an increase of FLuc under red light treatment while transfer to the dark or blue light led to termination of gene expression (faster and stronger under blue light). In addition, the latter samples (On-Off) were split after 6 h of blue light treatment further into blue and red light-incubation conditions (On-Off-On). We observed re-activation of gene expression, demonstrating the reversibility

of the system. Samples illuminated for the whole period (15 h) with blue light showed only background levels of expression. We normalized FLuc concentrations using the measured RLuc as in Experiment 1. Thus, the observation function of Experiment 2 becomes

$$\frac{\text{FLuc}_{\text{observed}}}{\text{RLuc}_{\text{observed}}} = \text{scale}_{\text{FLuc,Exp2}} [\text{FLuc}]. \quad (17)$$

Scaling factors are necessary to couple different measurements with relative scale in the same model. However, since the absolute scale of the relative FLuc concentration is unknown, the scaling factor of one FLuc measurement has to be set to one to avoid over-parametrization. Since all other FLuc measurements of Experiments 1 have a scaling factor, we set

$$\text{scale}_{\text{FLuc,Exp2}} = 1. \quad (18)$$

c. Experiment 3: Characterization of the system mRNA kinetics

In the third experiment (shown in **Extended Data Fig. 1b**) we measured a time series of the FLuc mRNA concentration. In brief, to determine mRNA kinetics, after transformation followed by 16 h of dark incubation, the protoplasts were illuminated for 4 h with red light and then transferred to blue light for additional 3 h. Samples were collected at the indicated time points and analyzed by RT-qPCR. We normalized the FLuc mRNA concentrations using the geometric mean (geomean) of the measured mRNA levels of EF and TIP41L housekeeping genes. We repeated the experiment twice with two technical replicates for each transcript per measurement. Both experiments were used for the parameterization. The observation function of repetition i is

$$\frac{\text{FLuc}_{\text{mRNA,observed}}}{\text{geomean}(\text{EF,TIP41L})_{\text{mRNA,observed}}} = \text{scale}_{\text{FLuc}_{\text{mRNA}},\text{Exp3,Rep}_i} [\text{FLuc}_{\text{mRNA}}]. \quad (19)$$

As discussed in Experiment 2, one of the two scaling factors can be set to one, because the absolute concentration of the normalized $\text{FLuc}_{\text{mRNA}}$ is unknown.

$$\text{scale}_{\text{FLuc}_{\text{mRNA}}, \text{Exp3}, \text{Rep}_1} = 1. \quad (20)$$

d. Experiment 4: Characterization of the system for different illumination times

In the fourth experiment (shown in **Supplementary Fig. 1a**) we measured the response of the system to different times of stimulation with red light from 0 to 12 h, with six replicates per measurement. Results of two independent representative experiments were used for the parameterization. We measured the FLuc concentration and normalized it with RLuc similarly to experiments 1 and 2. The observation function of repetition i of the two repetitions is

$$\frac{\text{FLuc}_{\text{observed}}}{\text{RLuc}_{\text{observed}}} = \text{scale}_{\text{FLuc}, \text{Exp4}, \text{Rep}_i} [\text{FLuc}]. \quad (21)$$

e. Experiment 5: Characterization of the system for different light intensities, “dose-response”

In the fifth experiment (shown in **Supplementary Fig. 1b,c**) we measured the response of the system to different blue and red light intensities, with six replicates per measurement. The observation function and normalization are similar to Experiments 1, 2 and 4:

$$\frac{\text{FLuc}_{\text{observed}}}{\text{RLuc}_{\text{observed}}} = \text{scale}_{\text{FLuc}, \text{Exp5}, \text{Color}} [\text{FLuc}]. \quad (22)$$

with the colour either being red or blue.

In these end point measurements and dose-response experiments (**Supplementary Fig. 1a,b**) we observed that as little as 15 min of $10 \mu\text{mol m}^{-2} \text{s}^{-1}$ red light treatment or very low intensities of red light ($0.25 \mu\text{mol m}^{-2} \text{s}^{-1}$ for 18 h) are sufficient to strongly activate expression. Similarly, the blue light dose-response study indicated that, while keeping the red illumination constant, blue light-mediated repression overrides red light-mediated activation effects (**Supplementary Fig. 1c**).

f. Initial conditions

The initial conditions of the LOV and PhyB complexes were set to

$$\text{LOV}_{\text{closed}}(0) = 1 \quad (23)$$

$$\text{LOV}_{\text{open}}(0) = 0 \quad (24)$$

$$\text{PhyB}_r(0) = 1 \quad (25)$$

$$\text{PhyB}_{\text{fr}}(0) = 0, \quad (26)$$

i.e. their inactive states, because before each experiment the system was left in the dark.

For the initial concentration of $\text{FLuc}_{\text{mRNA}}$ we assumed a steady state between the basal transcription of the mRNA and its degradation

$$\text{FLuc}_{\text{mRNA}}(0) = \frac{b_{\text{transcription}}}{k_{\text{deg,FLuc}_{\text{mRNA}}}}. \quad (27)$$

We estimated the initial concentration of FLuc together with the other model parameters as a model parameter:

$$FLuc(0) = \text{init}_{FLuc}. \quad (28)$$

g. Simplifications

Müller *et al.* 2013⁷ previously showed, that under far-red light the PhyB system is completely in the PhyB_r state. We incorporated this information in the model by setting

$$k_{\text{off,PhyB,farred}} = 100 \text{ h}^{-1}. \quad (29)$$

The ratios of the two complexes of Phytochrome B under red light (660 nm) and far-red light (740 nm) were calculated using the data of Kelly and Lagarias 1985⁸ according to Legris *et al.* (2016)⁹. They describe the ratio of PhyB_{fr} to the total PhyB population in these light conditions including the effects of the constant dark reversion $k_{\text{off,PhyB,dark}}$.

These ratios are

$$r_{\text{PhyB}_{fr},\text{red}} = \frac{[\text{PhyB}_{fr}]}{[\text{PhyB}_r] + [\text{PhyB}_{fr}]} = 0.728 \quad \text{at } 10 \mu\text{mol m}^{-2} \text{ s}^{-1} \text{ of red light,} \quad (30)$$

$$r_{\text{PhyB}_{fr},\text{farred}} = \frac{[\text{PhyB}_{fr}]}{[\text{PhyB}_r] + [\text{PhyB}_{fr}]} = 0.002 \quad \text{at } 10 \mu\text{mol m}^{-2} \text{ s}^{-1} \text{ of far-red light.} \quad (31)$$

Since the ratios were measured under constant red light intensity I_{red} and temperature, we assumed a quasi-steady state of the PhyB system. Thus, using the relation

$$\frac{[\text{PhyB}_{fr}]}{[\text{PhyB}_r]} = \frac{r_{\text{PhyB}_{fr},\text{red}}}{1 - r_{\text{PhyB}_{fr},\text{red}}} = K_{\text{PhyB}_{fr},\text{red}} \quad (32)$$

Eqs. (3) and (4) lead to

$$K_{\text{PhyB}_{\text{fr}},\text{red}} = \frac{-k_{\text{on,PhyB},\text{red}} I_{\text{red}} + k_{\text{off,PhyB},\text{red}} I_{\text{red}} K_{\text{PhyB}_{\text{fr}},\text{red}} + k_{\text{off,PhyB},\text{dark}} K_{\text{PhyB}_{\text{fr}},\text{red}}}{k_{\text{on,PhyB},\text{red}} \frac{I_{\text{red}}}{K_{\text{PhyB}_{\text{fr}},\text{red}}} - k_{\text{off,PhyB},\text{red}} I_{\text{red}} - k_{\text{off,PhyB},\text{dark}}}. \quad (33)$$

By algebraic calculation we obtain

$$k_{\text{on,PhyB},\text{red}} = \left(k_{\text{off,PhyB},\text{red}} + \frac{k_{\text{off,PhyB},\text{dark}}}{I_{\text{red}}} \right) K_{\text{PhyB}_{\text{fr}},\text{red}}. \quad (34)$$

Since the intensity $I_{\text{red}} = 10 \mu\text{mol m}^{-2} \text{s}^{-1}$ is known, this equation simplifies the model by one parameter, the On-rate of the PhyB complex in red light. An identical calculation was performed for the far-red rate $k_{\text{on,PhyB},\text{farred}}$.

h. Stoichiometric considerations for the B_{Off} and R_{On} components concentrations

The stoichiometry between the B_{Off} and the R_{On} components does not influence the system's behaviour. This can be concluded both from the computational model as well as from the experiments. In the computational model, a change in concentration of one of two systems corresponds to a change in the scaling parameters described in the previous sections. The system equations and reactions would remain unchanged and only the scaling parameter would encode the changed stoichiometric balance. This analysis is consistent with the experiments under varying experimental conditions that show that all relevant effects can be derived from the relative concentrations. Furthermore, it indicates that the stoichiometry between the two factors plays no role since their effects are uncorrelated. The B_{Off} complex inhibition of the transcription is independent of the R_{On} systems state, *i.e.* relative or absolute concentration.

5. Results of parameter estimation

The complete model including the observation functions of the experiments was fitted to 406 data points using the maximum likelihood approach. 25 parameters were estimated, of which one was an initial value, ten were dynamic parameters, nine were scaling parameters and five were error parameters.

We performed the numerical integration, fitting process and identifiability analysis with the profile likelihood method in MATLAB using the freely available Data2Dynamics software¹⁰. It uses the CVODES¹¹ solver to numerically integrate the ordinary differential equations. The parameter estimation was performed using the trust region algorithm LSQNONLIN¹². We optimized the parameter space in logarithmic space, thus naturally enabling a scan of the parameters over many orders of magnitude.

A thorough search for the global optimum requires multiple optimization runs with randomly sampled initial parameter sets. We thus performed 200 runs, of which 20 converged to the lowest minimum, suggesting that it is the global optimum (**Supplementary Fig. 9a**). Other local optima were found, but because they are significantly worse than the best optimum they are not included in the further analysis.

The identifiability analysis using the profile likelihood method showed two practically non-identifiable parameters (**Supplementary Fig. 10**). The two parameters describe the LOV systems inhibitory behaviour, *i.e.* $k_{on,LOV}$ describes the rate, at which LOV is created and $k_{inh,LOV}$ describes the inhibition strength of the LOV complex on the mRNA transcription. The practical non-identifiabilities in these two parameters stem from the fact, that the absolute concentration of LOV is unknown, thus the LOV concentration and its inhibition strength are symmetrically linked. A reduction of the model should thus fix one of the dynamic parameters. The inhibition strength is the natural choice since it has the unit of an inverse concentration.

After fixing the inhibition strength $k_{\text{inh,LOV}}$

$$k_{\text{inh,LOV}} = 25.04 \quad (35)$$

to the value of the global optimum, the previously described analysis pipeline was performed again on the reduced model with now 24 dynamic parameters.

From 200 runs, 97 converged to the lowest minimum, strongly indicating, that it is the global optimum (**Supplementary Fig. 9b**). One other local minimum was found, however, it was significantly worse than the lowest minimum. The profile likelihood analysis (**Supplementary Fig. 11**) shows, that all parameters are identifiable. The 95 % point-wise confidence intervals of the parameters are shown in **Supplementary Table 3**.

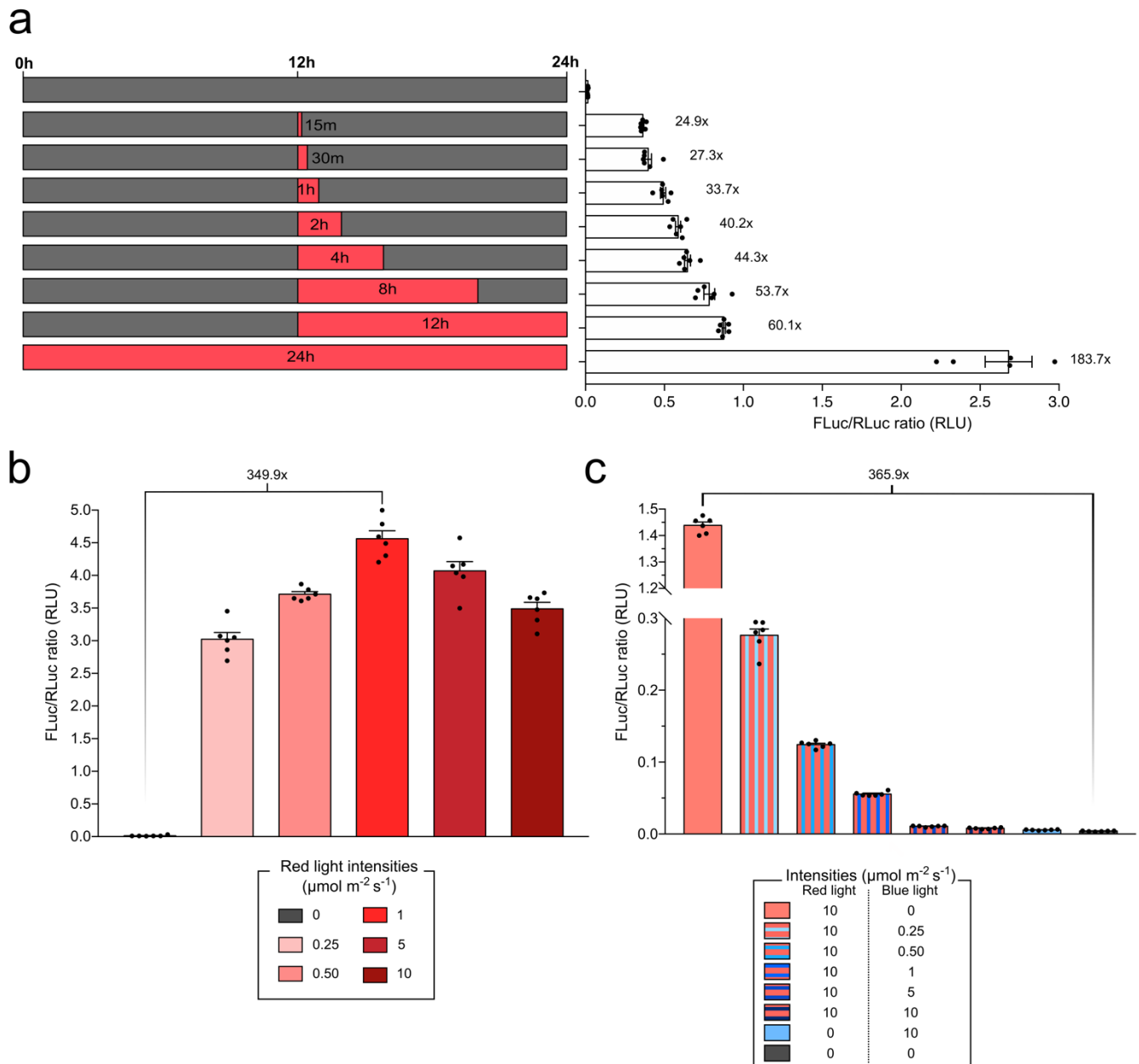
6. Characterization of the system by simulations and validation

We performed simulations to characterize the behaviour of the system under different light conditions. For this purpose we used the model, calibrated to the optimal parameter set with all data discussed in Section 4, *i.e.* the time-series mRNA and protein FLuc measurements (**Extended Data Fig. 1a,b, Supplementary Fig. 1a**) as well as light dose-response FLuc measurements (**Supplementary Fig. 1b,c**). **Extended Data Fig. 1c** shows a simulation of the normalized FLuc concentration from 0 to 18 h given different red light intensities as stimuli of the system in the absence of blue light. **Supplementary Fig. 2** shows a simulation of the normalized FLuc concentration given different red and blue light intensities after 12 h.

The above-mentioned characterization was validated by measuring the expression level of FLuc for different experimental conditions, *i.e.* red light intensities and illumination periods. For this, PULSE was transformed into protoplasts and kept 12 h in the dark prior to incubation under six different combinations of red light intensities and illumination durations selected from the heatmap (**Extended Data Fig. 1c**). These

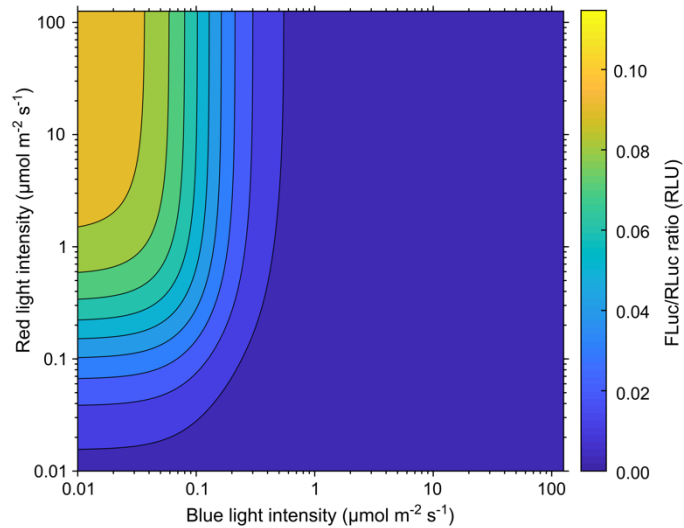
validation measurements were then compared to the model predictions, as can be seen in **Extended Data Fig. 1d**. The prediction uncertainty was determined by evaluating the prediction profile likelihood for each prediction, *i.e.* each experimental condition of the validation measurements¹³. There is a strong correspondence between predicted and experimental FLuc/RLuc determined values ($\chi^2 = 405.93$, $p = 0.18$) (**Extended Data Fig. 1d**), which indicates the applicability of the model to determine the experimental conditions (light intensity and time ranges) needed to achieve a tight control over the levels of gene expression with PULSE.

Supplementary Figures

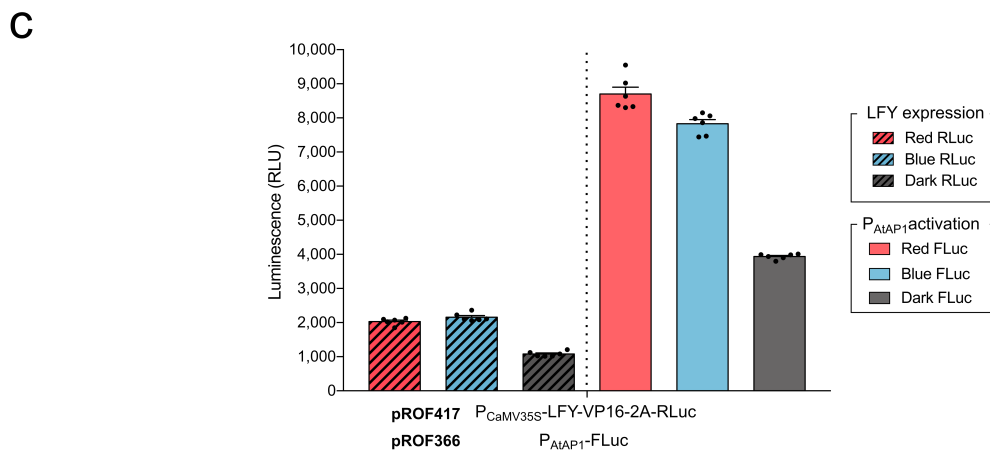
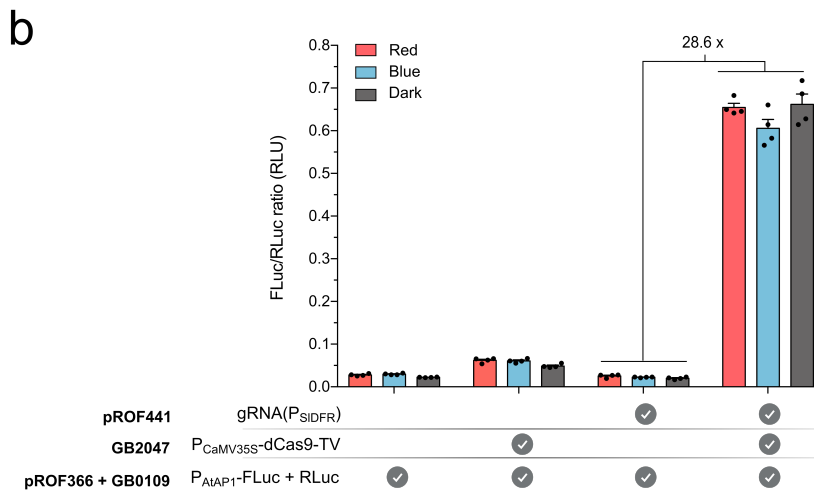
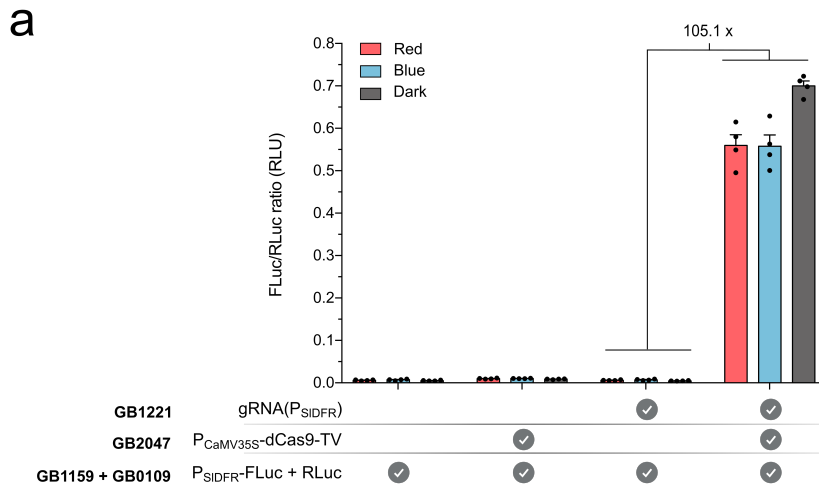


Supplementary Figure 1. Characterization of PULSE-driven FLuc expression in *Arabidopsis* protoplasts to calibrate the mathematical model. **(a)** End point FLuc kinetics with red light treatment of different durations, as indicated. Grey areas correspond to darkness treatment and red areas to $10 \mu\text{mol m}^{-2} \text{s}^{-1}$ of red light. **(b,c)** Dose-response of FLuc expression for different red light intensities (b) and constant red light with different blue light intensities treatments (c). FLuc was normalized to RLuc activity. Protoplasts were kept in darkness or illuminated with the indicated intensities of light for 18 h. **(a-c)** Mean and SEM are plotted, $n = 6$ protoplasts samples

for each condition. Indicated induction folds are relative to dark. RLU = Relative Luminescence Units. Representative experiments from two (b,c) to three (a) similar independent experiments.

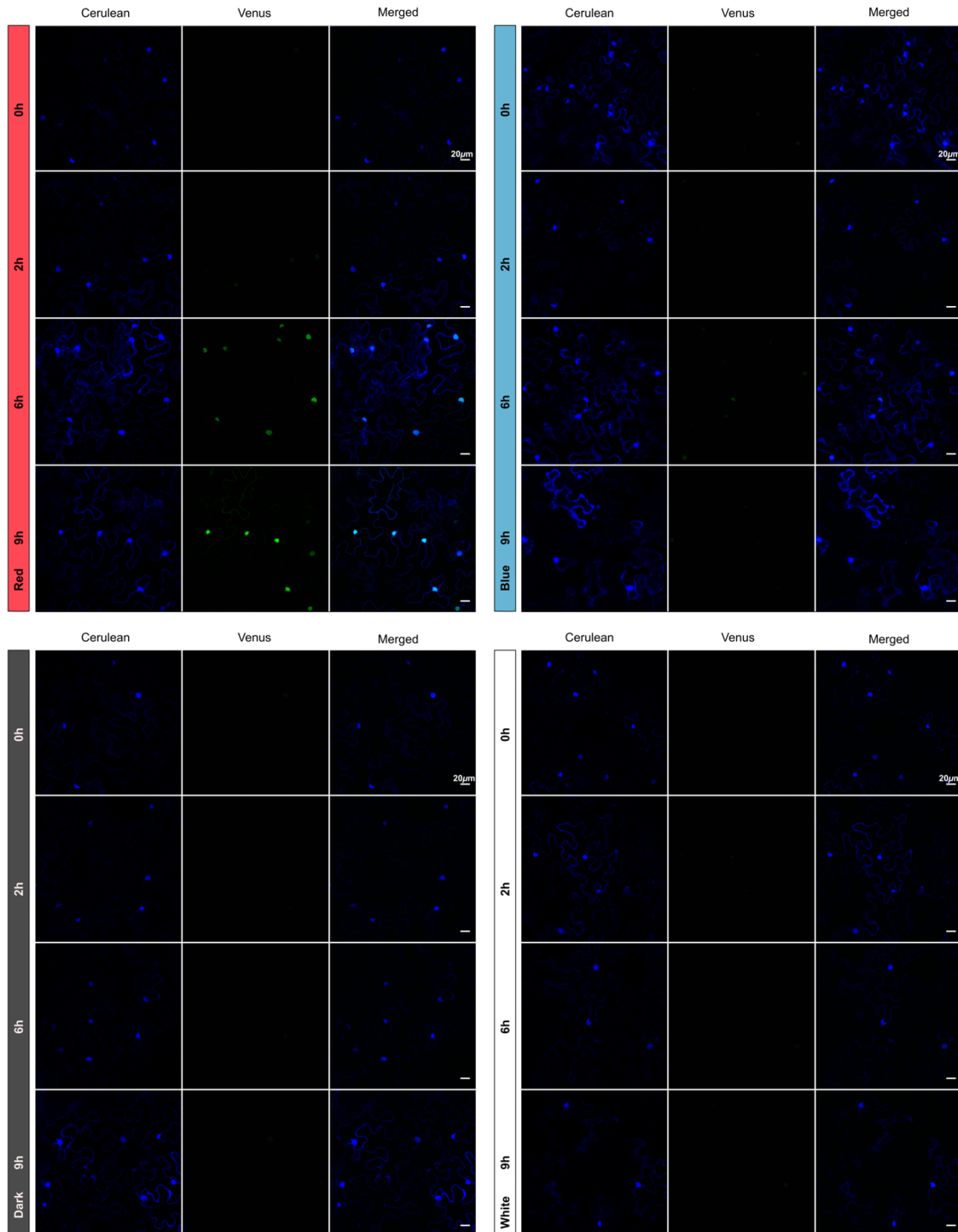


Supplementary Figure 2. Heatmap representation of the model predictions of PULSE-controlled protein expression levels as a function of light intensities. The calibrated model yields estimated FLuc/RLuc expression ranges under simultaneous illumination with a range of red and blue light intensities for 12 h.



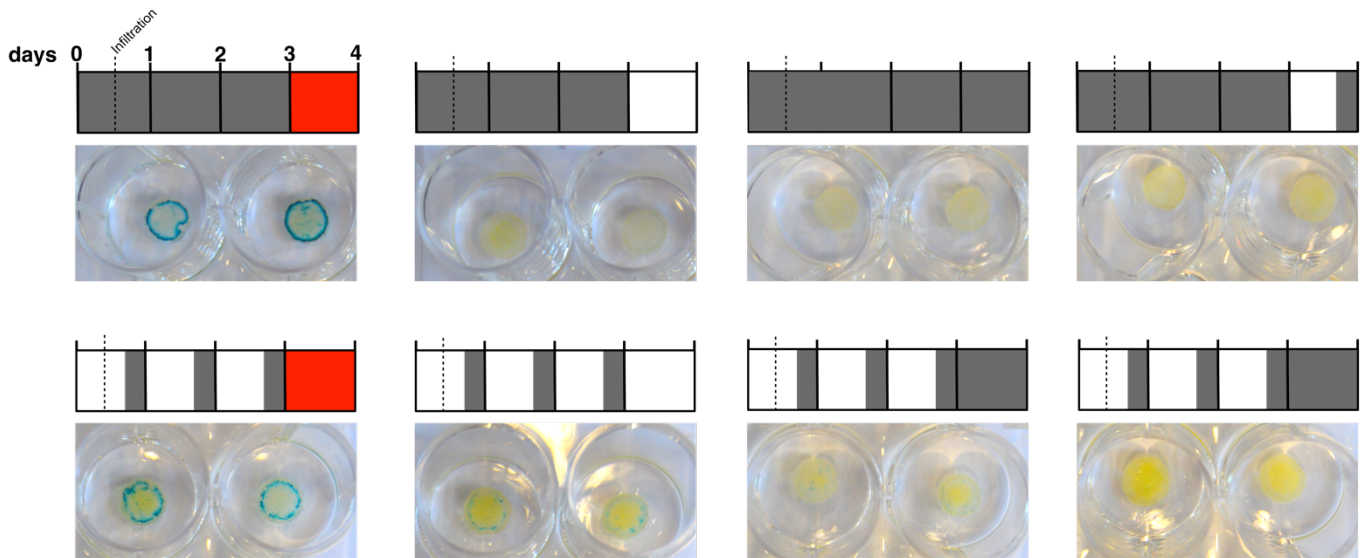
Supplementary Figure 3. Constitutive expression of a Cas9-derived gene activator (dCas9-TV) and an Arabidopsis transcription factor (LFY) in Arabidopsis protoplasts. **(a)** Normalized FLuc activity as a measure of SIDFR promoter activity under the indicated experimental conditions. **(b)** Normalized FLuc activity as a measure of AtAP1 promoter activation under the indicated experimental conditions. **(c)** RLuc

determination as proxy of LFY-VP16 expression (striped bars) and FLuc as a measure of P_{AtAP1} activation (solid bars). **(a-c)** FLuc and RLuc activities were determined 18 – 19 h after illumination. Protoplasts were kept in the dark, or illuminated with $10 \mu\text{mol m}^{-2} \text{s}^{-1}$ of red or blue light. Mean and SEM are plotted for FLuc/RLuc ratios of $n = 4$ protoplast samples (a,b), and luminescence of $n = 6$ protoplast samples with background values (configuration without $P_{CaMV35S}$ -LFY-VP16-2A-RLuc) subtracted for FLuc (c). RLU = Relative Luminescence Units. Representative experiments from two (a,c) and four (b) independent experiments.

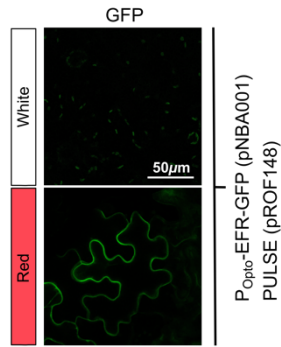


Supplementary Figure 4. Fluorescence confocal microscopy images from optogenetically controlled Venus and constitutive Cerulean expression in *Nicotiana benthamiana* leaves. Full set of images corresponding to the results shown in **Fig. 5a**. Plants transiently transformed with PULSE-driven Venus (pROF346) incubated for 2.5 d in dark were subjected for the indicated durations to light treatment of $10 \mu\text{mol m}^{-2} \text{s}^{-1}$

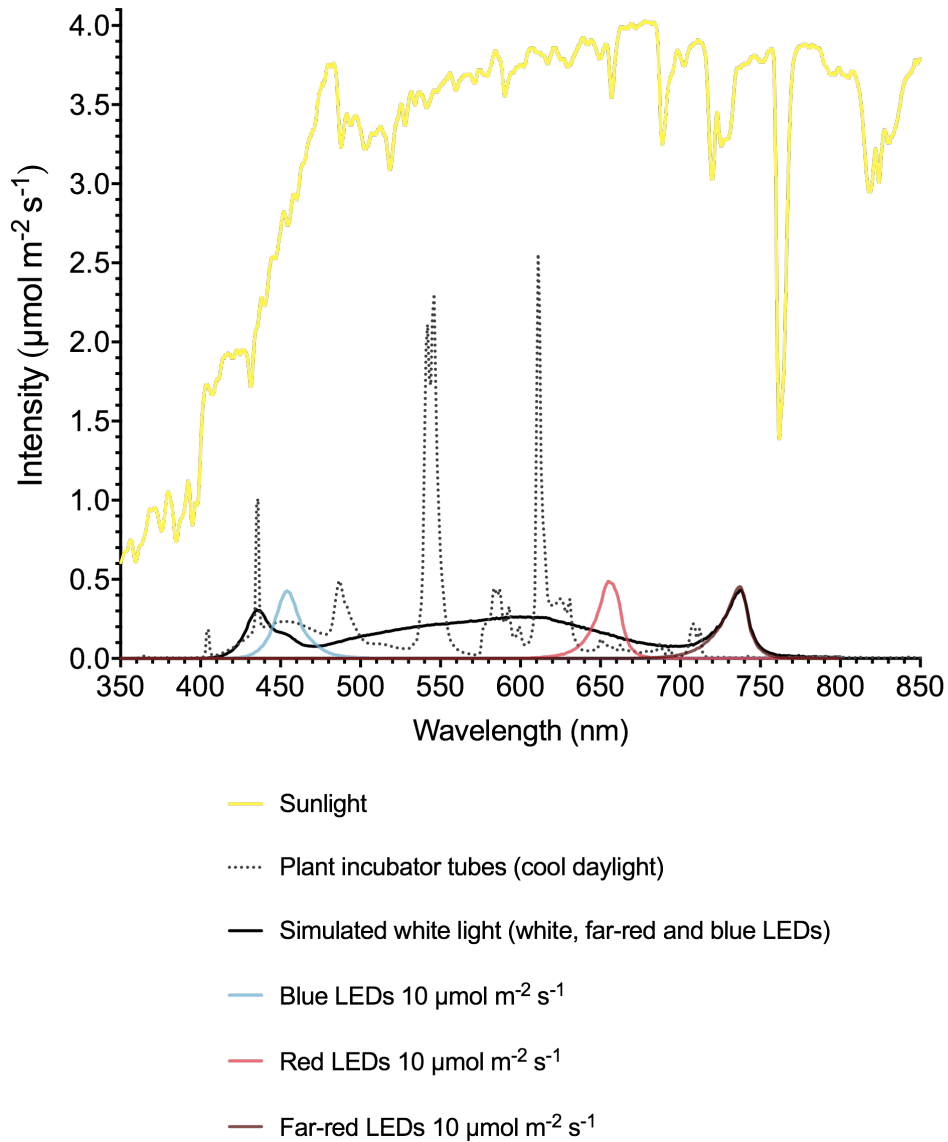
¹ red light, 10 $\mu\text{mol m}^{-2} \text{s}^{-1}$ blue light, white light, or darkness. Representative images of three independent experiments are shown.



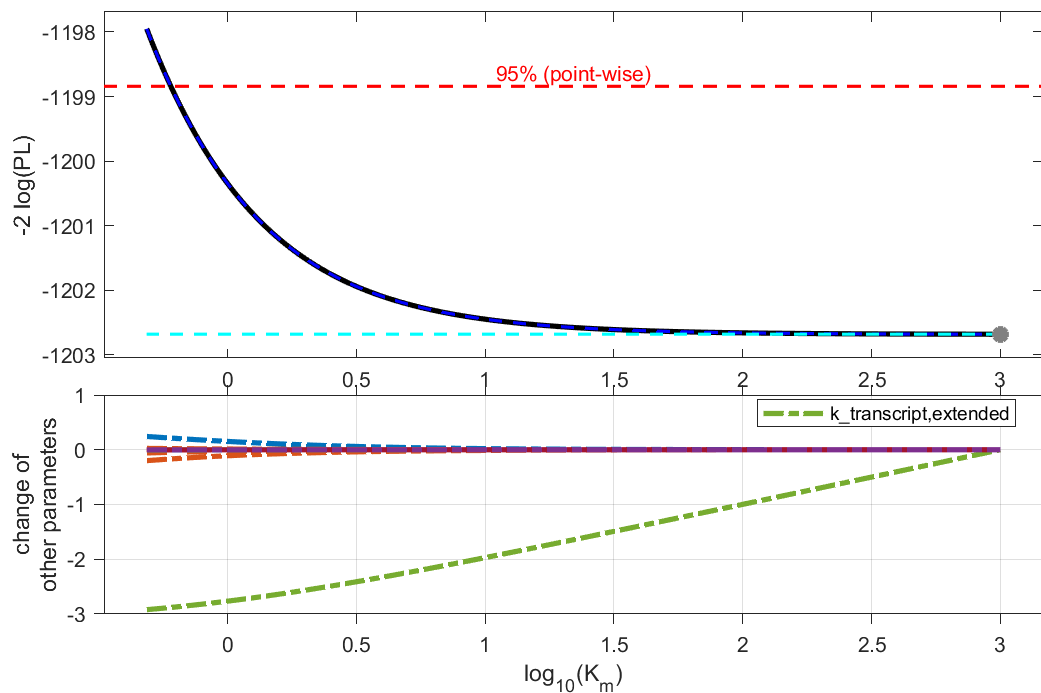
Supplementary Figure 5. Optogenetically controlled GUS expression in *N. benthamiana* leaves. Plants transiently transformed with PULSE-driven GUS (BM00369) were kept in darkness or a plant incubator for 2.5 d (16 h light - 8 h darkness) prior to illumination for 1 d with 10 $\mu\text{mol m}^{-2} \text{s}^{-1}$ red light, white light, or darkness, as indicated in the schemes. Two disks from different leaves with the same treatment were incubated with GUS staining solution. A representative experiment of two independent experiments is shown.



Supplementary Figure 6. Fluorescence confocal microscopy images of optogenetically controlled EFR-GFP under different light condition. Plants transiently transformed with PULSE-driven EFR-GFP (pNBA001) were incubated for 2 d prior to induction with $10 \mu\text{mol m}^{-2} \text{s}^{-1}$ red light for additional 16 h (white light treatment was used as control). This expression control corresponds to **Fig. 6b**. Shown are representative images of three independent experiments.

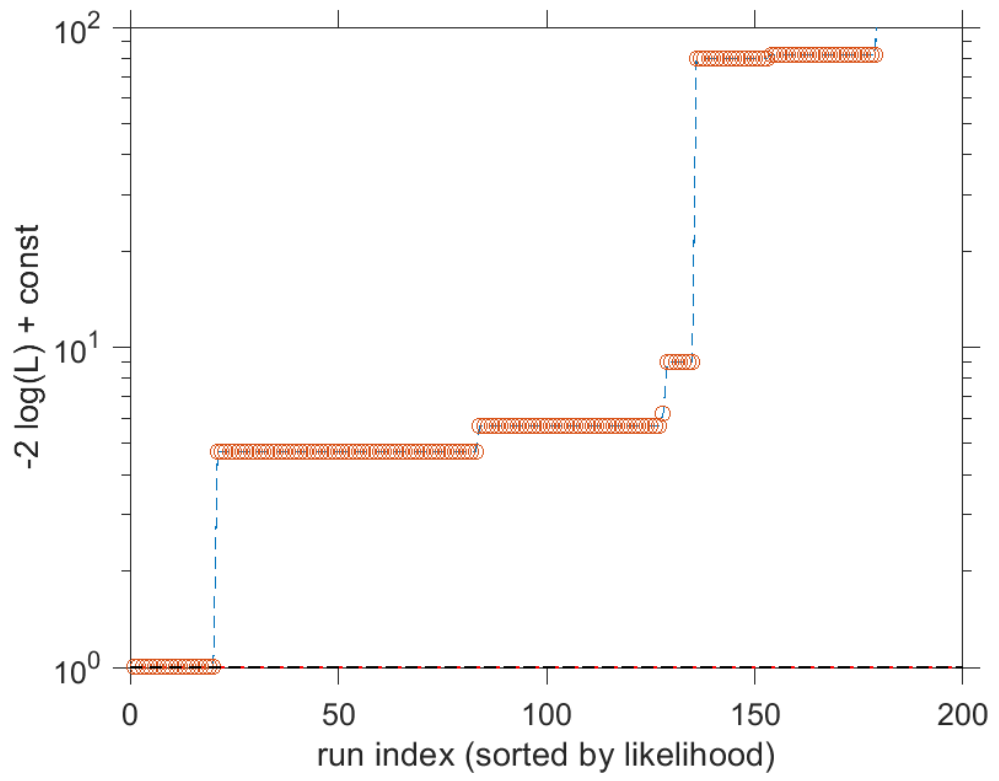


Supplementary Figure 7. Spectra of the LEDs used for the illumination treatments. Illumination treatments were performed with LED panels adjusted to intensities of 10 $\mu\text{mol m}^{-2} \text{s}^{-1}$ for the red (λ_{max} 655 nm), blue (λ_{max} 461 nm), or far-red (λ_{max} 740 nm). For the simulated white illumination treatments (continuous dark line), white, blue and far-red LEDs were used and the intensity was adjusted in order to have 10 $\mu\text{mol m}^{-2} \text{s}^{-1}$ of blue light 420-490 nm, red light 620-680 nm, and far-red light 700-750 nm (light ranges according to Sellaro *et al.* 2010)¹⁴. Discontinuous dark line corresponds to fluorescent tubes (cool daylight OSRAM). The sunlight spectrum (yellow line) is adapted from Casal¹⁵.

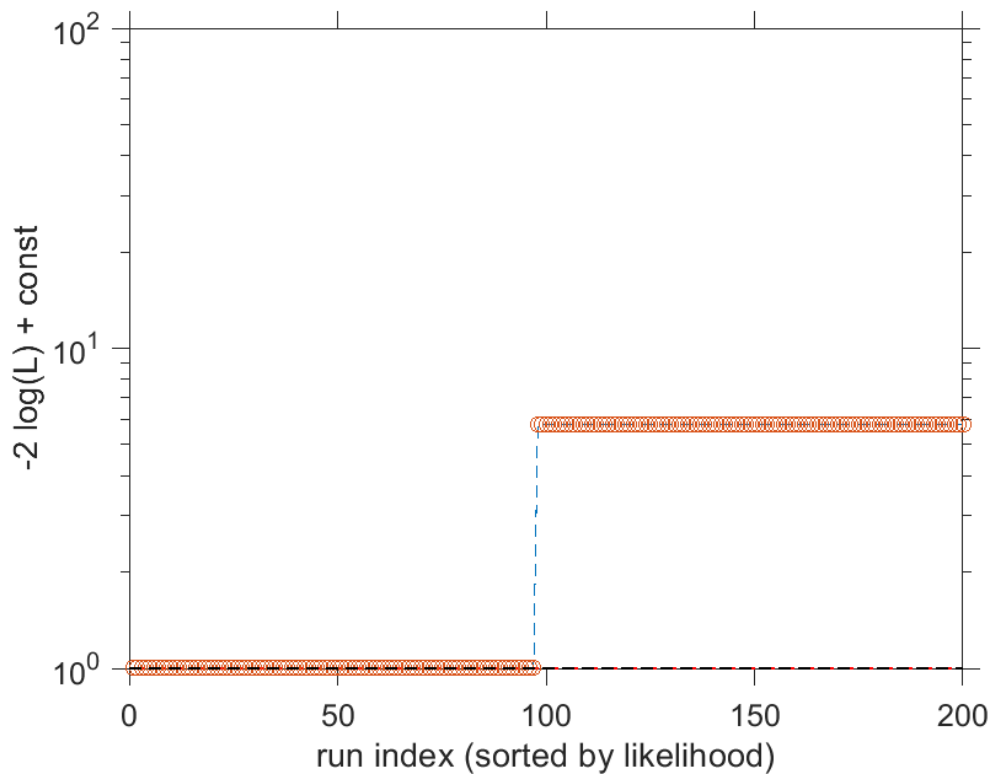


Supplementary Figure 8. Parameter profile likelihood of the non-identifiable parameter of the FLuc mRNA transcription when including saturation dynamics and changes in other parameters over the range of profile. The black lines show the profile likelihood, while the optimal parameter value is shown as a grey dot. The dashed red line indicates the 95 % confidence level. Its intersection points with the profile likelihood yield the point-wise 95 % confidence intervals of the parameter. The dashed blue lines indicates the $-2\log(\text{PL})$ value of the optimal parameter set. The parameter K_m is practically non-identifiable towards infinity, indicating that the Michaelis-Menten kinetics are in its linear limit, *i.e.* the saturation is not relevant to describe the data. The lower graph shows the changes in the other parameters in orders of magnitude over the range of the profile. It can clearly be seen, that K_m and $k_{\text{transcript,extended}}$ are linearly linked and their ratio constant over the entire parameter space.

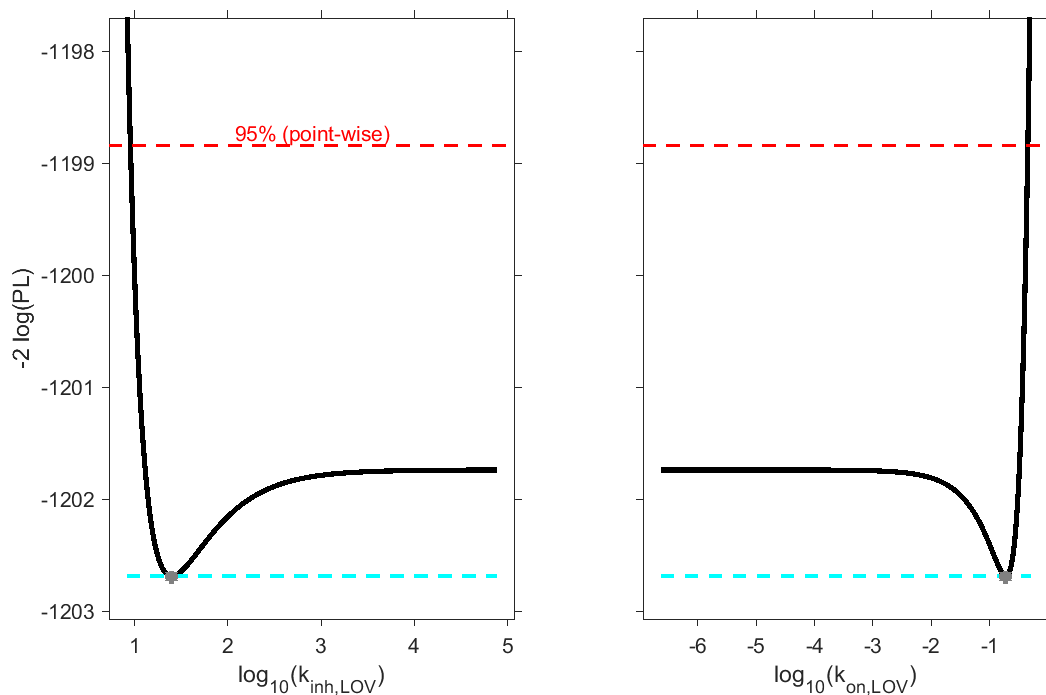
a



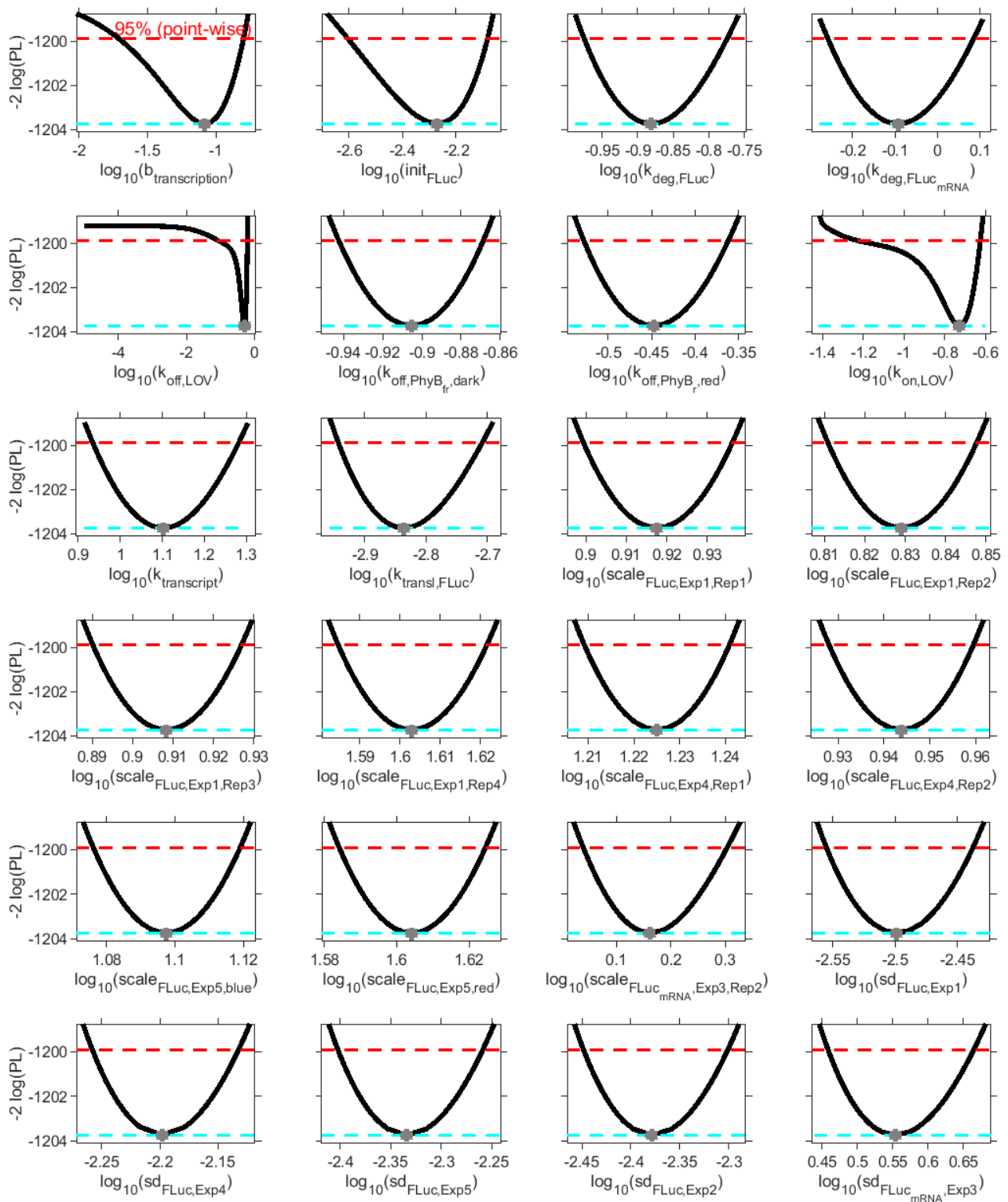
b



Supplementary Figure 9. Multiple optimization runs with random initial parameter guesses. **(a)** 200 optimization runs with random initial parameters sorted by the $-2 \log(L)$ value for the full model. The lowest minima were found in 20 of the runs. All other local minima are significantly higher than the lowest minima. **(b)** 200 optimization runs with random initial parameters sorted by the $-2 \log(L)$ value for the reduced model. The lowest minima were found in 97 of the runs. The other local minimum is significantly higher than the lowest minimum.



Supplementary Figure 10. Parameter profile likelihood of the two non-identifiable parameters of the full model. The black lines show the profile likelihood, while the optimal parameter value is shown as a grey dot. The dotted red line indicates the 95 % confidence level. Its intersection points with the profile likelihood yield the point-wise 95 % confidence intervals of the parameter. The dotted blue lines indicate the $-2 \log(\text{PL})$ value of the optimal parameter set.



Supplementary Figure 11. Parameter profile likelihood of the estimated parameters of the reduced model. The black lines show the profile likelihood, while the optimal parameter value is shown as a grey dot. The dotted red lines indicate the 95 % confidence level. Its intersection points with the profile likelihood yield the point-wise 95 % confidence intervals of the parameter. The dotted blue lines indicate the $-2 \log(\text{PL})$ value of the optimal parameter set. All parameters are identifiable, *i.e.* they have finite 95 % confidence intervals.

Supplementary Tables

Supplementary Table 1. Plasmids used in experiments in this work (grey shading). Plasmids below in the hierarchy were used as intermediate plasmids for cloning purposes. Arrows denote hierarchical dependence in the cloning process, e.g. BM00369 was constructed based on EC15029, BM00092, BM00093, BM00368, BM00367, EC41822. In turn, BM00092 was constructed using EC10991, and so on.

| Plasmid name | | Description | Insert | Backbone | Cloning procedure |
|--------------|---------|---|---|-----------------------|--|
| BM00369 | | T _{nos} -nptII-P _{nos} -T _{nos} -NLS-PIF6-E-P _{CaMV35S} -T _{nos} -dsRed-P _{AtUbi10} -T _{nos} -NLS-VP16-PhyB-P _{CaMV35S} -T _{nos} -EL222-NLS-SRDX-P _{CaMV35S} -T _{35S} -GUS-P _{hCMVmin} -(C120) ₅ -(etr) ₈ | EC15029, BM00092, EC15034 ¹⁶ , BM00093, BM00368, BM00367, EC41822 ¹⁶ | EC50505 ¹⁷ | Bpil restriction-ligation reaction (Golden Gate) |
| ↳ | EC15029 | P _{nos} -nptII-T _{nos} | EC15057, EC15068 (same sequence as nptII cassette from LucTrap-1 ¹⁸), EC41421 ¹⁶ | EC47802 ¹⁷ | Bsal restriction-ligation reaction (Golden Gate) |
| ↳ | BM00092 | P _{CaMV35S} -E-PIF6-NLS-T _{nos} | EC15058 ¹⁶ , EC10991, EC41421 ¹⁶ | EC47811 ¹⁷ | Bsal restriction-ligation reaction (Golden Gate) |
| ↳ | EC10991 | E-PIF6-NLS | E-PIF6-NLS was synthesized (same sequence as pMZ827 ¹⁹) and provided in a Golden Gate L0 plasmid | EC41308 ¹⁷ | Bpil restriction-ligation reaction (Golden Gate) |
| ↳ | EC15034 | P _{AtUbi10} -dsRed-T _{nos} ¹⁶ | | | |
| ↳ | BM00093 | P _{CaMV35S} -PhyB-VP16-NLS-T _{nos} | EC15058 ¹⁶ , EC10992, EC41421 ¹⁶ | EC47831 ¹⁷ | Bsal restriction-ligation reaction (Golden Gate) |
| ↳ | EC10992 | PhyB-VP16-NLS | PhyB-VP16-NLS was synthesized (same sequence as pMZ828 ¹⁹) and provided in a Golden Gate L0 plasmid | EC41308 ¹⁷ | Bpil restriction-ligation reaction (Golden Gate) |
| ↳ | BM00368 | P _{CaMV35S} -SRDX-NLS-EL222-T _{nos} | EC15058 ¹⁶ , BM00103, EC41421 ¹⁶ | EC47841 ¹⁷ | Bsal restriction-ligation reaction (Golden Gate) |
| ↳ | BM00103 | SRDX-NLS-EL222 | SRDX-NLS-EL222 was amplified from pROF051 with oligos oBM0080 and oBM0081 | EC41308 ¹⁷ | Bpil restriction-ligation reaction (Golden Gate) |

| | | | | | |
|---------|---------|--|--|-----------------------|--|
| ↳ | BM00367 | (etr) ₈ -(C120) ₅ -P _{hCMVmin} -GUS-T _{35S} | BM00102, EC75111 ¹⁶ , EC41414 ¹⁶ | EC47852 ¹⁷ | Bsal restriction-ligation reaction (Golden Gate) |
| ↳ | BM00102 | (etr) ₈ -(C120) ₅ -P _{hCMVmin} | (etr) ₈ -(C120) ₅ -P _{hCMVmin} was amplified from pROF021 with oligos oBM0083 and oBM0079 | EC41295 ¹⁷ | Bpil restriction-ligation reaction (Golden Gate) |
| BM00654 | | T _{nos} -nptII-P _{nos} -T _{nos} -NLS-PIF6-E-P _{CaMV35S(short)} -T _{nos} -AsiSI-RLuc-Nrul-P _{AtUbi10} -T _{nos} -NLS-VP16-PhyB-P _{CaMV35S(short)} -T _{nos} -EL222-NLS-SRDX- P _{CaMV35S(short)} -T _{35S} -Sbfl-FLuc-Spel-P _{hCMVmin} -(C120) ₅ -(etr) ₈ | EC15029, BM00092, BM00644, BM00093, BM00368, BM00643, EC41822 ¹⁶ | EC50505 ¹⁷ | Bpil restriction-ligation reaction (Golden Gate) |
| ↳ | EC15029 | P _{nos} -nptII-T _{nos} | EC15057, EC15068 (same sequence as nptII cassette from LucTrap-1 ¹⁸), EC41421 ¹⁶ | EC47802 ¹⁷ | Bsal restriction-ligation reaction (Golden Gate) |
| ↳ | BM00092 | P _{CaMV35S(short)} -E-PIF6-NLS-T _{nos} | EC15058 ¹⁶ , EC10991, EC41421 ¹⁶ | EC47811 ¹⁷ | Bsal restriction-ligation reaction (Golden Gate) |
| ↳ | EC10991 | E-PIF6-NLS | E-PIF6-NLS was synthesized (same sequence as pMZ827 ¹⁹) and provided in a Golden Gate L0 plasmid | EC41308 ¹⁷ | Bpil restriction-ligation reaction (Golden Gate) |
| ↳ | BM00644 | P _{AtUbi10} -Nrul-RLuc-AsiSI-T _{nos} | EC15062 ¹⁶ , BM00646, EC41421 ¹⁶ | EC47822 ¹⁷ | Bsal restriction-ligation reaction (Golden Gate) |
| ↳ | BM00646 | Nrul-RLuc-AsiSI | Nrul-RLuc-AsiSI was amplified from EC15806 ¹⁶ with oligos oBM0207 and oBM0208 | EC41308 ¹⁷ | Bpil restriction-ligation reaction (Golden Gate) |
| ↳ | BM00093 | P _{CaMV35S(short)} -PhyB-VP16-NLS-T _{nos} | EC15058 ¹⁶ , EC10992, EC41421 ¹⁶ | EC47831 ¹⁷ | Bsal restriction-ligation reaction (Golden Gate) |
| ↳ | EC10992 | PhyB-VP16-NLS | PhyB-VP16-NLS was synthesized (same sequence as pMZ828 ¹⁹) and provided in a Golden Gate L0 plasmid | EC41308 ¹⁷ | Bpil restriction-ligation reaction (Golden Gate) |
| ↳ | BM00368 | P _{CaMV35S(short)} -SRDX-NLS-EL222-T _{nos} | EC15058 ¹⁶ , BM00103, EC41421 ¹⁶ | EC47841 ¹⁷ | Bsal restriction-ligation reaction (Golden Gate) |
| ↳ | BM00103 | SRDX-NLS-EL222 | SRDX-NLS-EL222 was amplified from pROF051 with oligos oBM0080 and oBM0081 | EC41308 ¹⁷ | Bpil restriction-ligation reaction (Golden Gate) |
| ↳ | BM00643 | (etr) ₈ -(C120) ₅ -P _{hCMVmin} -SpeI-FLuc-Sbfl-T _{35S} | BM00102, BM00645, EC41414 ¹⁶ | EC47852 ¹⁷ | Bsal restriction-ligation reaction (Golden Gate) |

| | | | | | |
|---------|---------|---|---|-------------------------|---|
| ↳ | BM00102 | (etr) ₈ -(C120) ₅ -P _{hCMVmin} | (etr) ₈ -(C120) ₅ -P _{hCMVmin} was amplified from pROF021 with oligos oBM0083 and oBM0079 | EC41295 ¹⁷ | Bpil restriction-ligation reaction (Golden Gate) |
| ↳ | BM00645 | SpeI-FLuc-SbfI | SpeI-FLuc-SbfI was amplified from EC15217 ¹⁶ with oligos oBM0205 and oBM0206 | EC41308 ¹⁷ | Bpil restriction-ligation reaction (Golden Gate) |
| GB0109 | | P _{CaMV35S} -RLuc-T _{nos} ²⁰ | | | |
| GB1159 | | P _{SIDFR} -FLuc-T _{nos} ²¹ | | | |
| GB1221 | | P _{AtU6-26} -gRNA(P _{SIDFR})-sgRNA ²¹ | | | |
| GB2047 | | P _{CaMV35S} -dCas9-TV-T _{nos} ²¹ | | | |
| pMZ827 | | P _{CaMV35S} -E-PIF6(1-100)-NLS-T _{SV40} ¹⁹ | | | |
| pMZ828 | | P _{CaMV35S} -PhyB(1-650)-VP16-NLS-T _{SV40} ¹⁹ | | | |
| pNBA001 | | (etr) ₈ -(C120) ₅ -P _{hCMVmin} -EFR-GFP-T _{35S} | pNBA004, pNBA005, GFP ²² , T _{35S} ²² | Xpre2-S ²² | Bsal restriction-ligation reaction (Golden Gate) |
| ↳ | pNBA004 | (etr) ₈ -(C120) ₅ -P _{hCMVmin} | (etr) ₈ -(C120) ₅ -P _{hCMVmin} was amplified from pROF021 with oligos oNBA160/oNBA176 | CloneJET (ThermoFisher) | Blunt end cloning of PCR product with T4 DNA ligase |
| ↳ | pNBA005 | EFR | EFR was amplified from pNBA003 with oligos oNBA289/oNBA290 | CloneJET (ThermoFisher) | Blunt end cloning of PCR product with T4 DNA ligase |
| pNBA002 | | (etr) ₈ -(C120) ₅ -P _{hCMVmin} -GBP-mCherry-T _{35S} | pNBA004, pNBA006, T _{35S} ²² | Xpre2-S ²² | Bsal restriction-ligation reaction (Golden Gate) |
| ↳ | pNBA004 | (etr) ₈ -(C120) ₅ -P _{hCMVmin} | (etr) ₈ -(C120) ₅ -P _{hCMVmin} was amplified from pROF021 with oligos oNBA160/oNBA176 | CloneJET (ThermoFisher) | Blunt end cloning of PCR product with T4 DNA ligase |
| ↳ | pNBA006 | GBP-mCherry | GBP was synthesized (plant codon optimized sequence ²³) with Bsal overhangs and assembled to mCherry ²² by Bsal restriction-ligation reaction. The product was amplified with oligos oNBA145/oNBA146 | pUC57 ²² | Bpil restriction-ligation reaction (Golden Gate) |
| pNBA003 | | P _{CaMV35S} -EFR-GFP-T _{OCS} ²⁴ | | | |

| | | | | |
|-----------|---|---|--|--|
| pROF018 | $P_{CaMV35S}$ -NLS-KRAB-EL222- T_{nos} | NLS-KRAB-EL222 was amplified from pKM565 ²⁵ with oligos oROF023/oROF024. | pMZ827 ¹⁹ digested with NdeI/EcoRI | Gibson assembly of backbone and PCR insert |
| pROF021 | (etr) ₈ -(C120) ₅ -P _{hCMVmin} -FLuc-T _{SV40} | FLuc was excised from pMZ836 ¹⁹ with NotI/EcoRI | pROF020 digested with EcoRI/NotI | Ligation with T4 DNA ligase |
| ↳ pROF020 | (etr) ₈ -(C120) ₅ -P _{hCMVmin} -SEAP-T _{SV40} | (C120) ₅ was amplified from pGL4.32-C120-FLuc ²⁶ with oligos oROF027/oROF028. | pKM081 ²⁷ digested with NheI | Ligation with T4 DNA ligase |
| pROF050 | $P_{CaMV35S}$ -BRD-NLS-EL222- T_{nos} | NLS-linker-EL222 was amplified from pVP-EL222 ²⁶ with oligos oROF068/oROF024. BRD was added in a second PCR step with oligos oROF069/oROF024. | pMZ827 ¹⁹ digested with NdeI/EcoRI. | Gibson assembly of backbone and second PCR insert |
| pROF051 | $P_{CaMV35S}$ -SRDX-NLS-EL222- T_{nos} | NLS-linker-EL222 was amplified from pVP-EL222 ²⁶ with oligos oROF068/oROF024. SRDX was added in a second PCR step with oligos oROF070/oROF024. | pMZ827 ¹⁹ digested with NdeI/EcoRI. | Gibson assembly of backbone and second PCR insert |
| pROF141 | $P_{AtUbi10}$ -SRDX-NLS-EL222- T_{nos} _SF_ $P_{AtUbi10}$ -E-PIF6-NLS- T_{nos} _P $P_{AtUbi10}$ -PhyB-VP16-NLS- T_{nos} | pROF121, pROF120 | pDGB 1alpha ²⁰ | BsaI restriction-ligation reaction (GB) |
| ↳ pROF121 | $P_{AtUbi10}$ -SRDX-NLS-EL222- T_{nos} _SF | pROF117, <u>GB0107</u> ²⁰ | pDGB 1omega ¹²⁰ | BsmBI restriction-ligation reaction (GB) |
| ↳ pROF117 | $P_{AtUbi10}$ -SRDX-NLS-EL222- T_{nos} | <u>GB0223</u> ²⁰ , pROF081, <u>GB0037</u> ²⁰ | pDGB 1alpha ¹²⁰ | BsaI restriction-ligation reaction (GB) |
| ↳ pROF081 | SRDX-NLS-linker-EL222 (Pos. B3-B5) | The SRDX-NLS-linker-EL222 was amplified from pROF051 in two fragments in order to domesticate an internal restriction site. Patch A with oligos oROF095/oROF091, and Patch B with oligos oROF092/oROF093. | pUPD ²⁰ | BsmBI restriction-ligation reaction (GB) of Patch A, PatchB and pUPD |

| | | | | | |
|---------|---------|--|--|-----------------------------|---|
| ↳ | pROF120 | P _{AtUbi10} -E-PIF6-NLS-T _{nos} _P _{AtUbi10} -PhyB-VP16-NLS-T _{nos} | pROF104, pROF105 | pDGB 1omega2 ²⁰ | BsmBI restriction-ligation reaction (GB) |
| ↳ | pROF104 | P _{AtUbi10} -E-PIF6-NLS-T _{nos} | <u>GB0223</u> ²⁰ , pROF098, <u>GB0037</u> ²⁰ | pDGB 1alpha1 ²⁰ | BsaI restriction-ligation reaction (GB) |
| ↳ | pROF098 | E-PIF6-NLS (Pos. B3-B5) | E-PIF6-NLS was amplified from pMZ827 ¹⁹ with oligos oROF100/oROF101 | pUPD ²⁰ | BsmBI restriction-ligation reaction (GB) |
| ↳ | pROF105 | P _{AtUbi10} -PhyB-VP16-NLS-T _{nos} | <u>GB0223</u> ²⁰ , pMVV003, <u>GB0037</u> ²⁰ | pDGB 1alpha2 ²⁰ | BsaI restriction-ligation reaction (GB) |
| ↳ | pMVV003 | PhyB-VP16-NLS (Pos. B3-B5) | PhyB-VP16-NLS was amplified from from pMZ828 ¹⁹ | pUPD ²⁰ | BsmBI restriction-ligation reaction (GB) |
| pROF148 | | T _{nos} -nptII-P _{nos} _P _{AtUbi10} -SRDX-NLS-EL222-T _{nos} _P _{AtUbi10} -E-PIF6-NLS-T _{nos} _P _{AtUbi10} -PhyB-VP16-NLS-T _{nos} | pROF136, pROF120 | pDGB 1alpha2 ²⁰ | BsaI restriction-ligation reaction (GB) |
| ↳ | pROF136 | T _{nos} -nptII-P _{nos} _P _{AtUbi10} -SRDX-NLS-EL222-T _{nos} | pROF124, pROF103 | pDGB 1omega1 ²⁰ | BsmBI restriction-ligation reaction (GB) |
| ↳ | pROF124 | P _{nos} -nptII-T _{nos} | <u>GB0034</u> (gbccloning.org) | pDGB 1alpha1R ²⁰ | BsaI restriction-ligation reaction (GB) |
| ↳ | pROF103 | P _{AtUbi10} -SRDX-NLS-EL222-T _{nos} | <u>GB0223</u> ²⁰ , pROF081, <u>GB0037</u> ²⁰ | pDGB 1alpha2 ²⁰ | BsaI restriction-ligation reaction (GB) |
| ↳ | pROF081 | SRDX-NLS-linker-EL222 (Pos. B3-B5) | The SRDX-NLS-linker-EL222 was amplified from pROF051 in two fragments in order to domesticate an internal restriction site. Patch A with oligos oROF095/oROF091, and Patch B with oligos oROF092/oROF093 | pUPD ²⁰ | BsmBI restriction-ligation reaction (GB) of Patch A, Patch B and pUPD |
| ↳ | pROF120 | P _{AtUbi10} -E-PIF6-NLS-T _{nos} _P _{AtUbi10} -PhyB-VP16-NLS-T _{nos} | pROF104, pROF105 | pDGB 1omega2 ²⁰ | BsmBI restriction-ligation reaction (GB) |
| ↳ | pROF104 | P _{AtUbi10} -E-PIF6-NLS-T _{nos} | <u>GB0223</u> ²⁰ , pROF098, <u>GB0037</u> ²⁰ | pDGB 1alpha1 ²⁰ | BsaI restriction-ligation reaction (GB) |
| ↳ | pROF098 | E-PIF6-NLS (Pos. B3-B5) | E-PIF6-NLS was amplified from pMZ827 ¹⁹ with oligos oROF100/oROF101 | pUPD ²⁰ | BsmBI restriction-ligation reaction |

| | | | | | |
|---------|---------|--|--|----------------------------------|--|
| ↳ | pROF105 | P _{AtUbi10} -PhyB-VP16-NLS-T _{nos} | <u>GB0223</u> ²⁰ , pMVV003, <u>GB0037</u> ²⁰ | pDGB 1alpha2 ²⁰ | BsaI restriction-ligation reaction (GB) |
| ↳ | pMVV003 | PhyB-VP16-NLS (Pos. B3-B5) | PhyB-VP16-NLS was amplified from from pMZ828 ¹⁹ | pUPD ²⁰ | BsmBI restriction-ligation reaction (GB) |
| pROF346 | | T _{nos} -nptII-P _{nos} -T _{nos} -NLS-PIF6-E-P _{AtUbi10} -T _{nos} -AsiSI-NLS-Cerulean-Nrul-P _{AtUbi10(short)} -T _{nos} -NLS-VP16-PhyB- P _{AtUbi10} -T _{nos} -EL222-NLS-SRDX- P _{AtUbi10} -T _{35S} -Sbfl-H2B-Venus-Spel-P _{hCMVmin} -(C120) ₅ -(etr) ₈ | Venus-H2B was amplified from pAB146 with oligos oROF436/oROF442 | pROF345 digested with SpeI/SbfI | Gibson assembly of backbone and PCR insert |
| ↳ | pAB146 | attR2-Venus-H2B-T _{3A} ²⁸ | | | |
| ↳ | pROF345 | T _{nos} -nptII-P _{nos} -T _{nos} -NLS-PIF6-E-P _{AtUbi10} -T _{nos} -AsiSI-NLS-Cerulean-Nrul-P _{AtUbi10(short)} -T _{nos} -NLS-VP16-PhyB- P _{AtUbi10} -T _{nos} -EL222-NLS-SRDX- P _{AtUbi10} -T _{35S} -Sbfl-FLuc-Spel-P _{hCMVmin} -(C120) ₅ -(etr) ₈ | Cerulean-NLS was amplified from pAPB131 with oligos oROF415/oROF417 | BM00655 digested with Nrul/AsiSI | Gibson assembly of backbone and PCR insert |
| ↳ | pAPB131 | attR2-Cerulean-T _{3A} ²⁸ | | | |
| ↳ | BM00655 | T _{nos} -nptII-P _{nos} -T _{nos} -NLS-PIF6-E-P _{AtUbi10(short)} -T _{nos} -AsiSI-RLuc-Nrul-P _{AtUbi10} -T _{nos} -NLS-VP16-PhyB-P _{AtUbi10} -T _{nos} -EL222-NLS-SRDX-P _{AtUbi10(short)} -T _{35S} -Sbfl-FLuc-Spel-P _{hCMVmin} -(C120) ₅ -(etr) ₈ | EC15029, BM00648, BM00644, BM00649, BM00650, BM00643, EC41822 ¹⁶ | EC50505 ¹⁷ | Bpil restriction-ligation reaction (Golden Gate) |
| ↳ | EC15029 | P _{nos} -nptII-T _{nos} | EC15057, EC15068 (same sequence as nptII cassette from LucTrap-1 ¹⁸), EC41421 ¹⁶ | EC47802 ¹⁷ | BsaI restriction-ligation reaction (Golden Gate) |
| ↳ | BM00648 | P _{AtUbi10(short)} -E-PIF6-NLS-T _{nos} | BM00647, EC10991, EC41421 ¹⁶ | EC47811 ¹⁷ | BsaI restriction-ligation reaction (Golden Gate) |
| ↳ | BM00647 | P _{AtUbi10(short)} | P _{AtUbi10(short)} was amplified from EC15062 ¹⁶ using oligos oBM0209 and oBM0210 | EC41295 ¹⁷ | Bpil restriction-ligation reaction (Golden Gate) |
| ↳ | EC10991 | E-PIF6-NLS | E-PIF6-NLS was synthesized (same sequence as pMZ827 ¹⁹) and provided in a Golden Gate L0 plasmid | EC41308 ¹⁷ | Bpil restriction-ligation reaction (Golden Gate) |

| | | | | | |
|---------|---------|---|--|-----------------------------------|--|
| ↳ | BM00644 | P _{AtUbi10} -NruI-RLuc-AsiSI-T _{nos} | EC15062 ¹⁶ , BM00646, EC41421 ¹⁶ | EC47822 ¹⁷ | BsaI restriction-ligation reaction (Golden Gate) |
| ↳ | BM00646 | NruI-RLuc-AsiSI | NruI-RLuc-AsiSI was amplified from EC15806 ¹⁶ with oligos oBM0207 oBM0208 | EC41308 ¹⁷ | BpiI restriction-ligation reaction (Golden Gate) |
| ↳ | BM00649 | P _{AtUbi10(short)} -PhyB-VP16-NLS-T _{nos} | BM00647, EC10992, EC41421 ¹⁶ | EC47831 ¹⁷ | BsaI restriction-ligation reaction (Golden Gate) |
| ↳ | BM00647 | P _{AtUbi10(short)} | P _{AtUbi10(short)} was amplified from EC15062 ¹⁶ using oligos oBM0209 and oBM0210 | EC41295 ¹⁷ | BpiI restriction-ligation reaction (Golden Gate) |
| ↳ | EC10992 | PhyB-VP16-NLS | PhyB-VP16-NLS was synthesized (same sequence as pMZ828 ¹⁹) and provided in a Golden Gate L0 plasmid | EC41308 ¹⁷ | BpiI restriction-ligation reaction (Golden Gate) |
| ↳ | BM00650 | P _{AtUbi10(short)} -SRDX-NLS-EL222-T _{nos} | BM00647, BM00103, EC41421 ¹⁶ | EC47841 ¹⁷ | BsaI restriction-ligation reaction (Golden Gate) |
| ↳ | BM00647 | P _{AtUbi10(short)} | P _{AtUbi10(short)} was amplified from EC15062 ¹⁶ using oligos oBM0209 and oBM0210 | EC41295 ¹⁷ | BpiI restriction-ligation reaction (Golden Gate) |
| ↳ | BM00103 | SRDX-NLS-EL222 | SRDX-NLS-EL222 was amplified from pROF051 with oligos oBM0080 and oBM0081 | BM00103 | SRDX-NLS-EL222 |
| ↳ | BM00643 | (etr) ₈ -(C120) ₅ -P _{hCMVmin} -SpeI-FLuc-SbfI-T _{35S} | BM00102, BM00645, EC41414 ¹⁶ | EC47852 ¹⁷ | BsaI restriction-ligation reaction (Golden Gate) |
| ↳ | BM00102 | (etr) ₈ -(C120) ₅ -P _{hCMVmin} | (etr) ₈ -(C120) ₅ -P _{hCMVmin} was amplified from pROF021 with oligos oBM0083 and oBM0079 | EC41295 ¹⁷ | BpiI restriction-ligation reaction (Golden Gate) |
| ↳ | BM00645 | SpeI-FLuc-SbfI | SpeI-FLuc-SbfI was amplified from EC15217 ¹⁶ with oligos oBM0205 oBM0206 | EC41308 ¹⁷ | BpiI restriction-ligation reaction (Golden Gate) |
| pROF366 | | P _{AtAP1} -FLuc-T _{SV40} | P _{AtAP1} was amplified from Arabidopsis genomic DNA with oligos oROF401/403 | pROF021 digested with PstI/ EcoRI | Gibson assembly of backbone and PCR insert |
| pROF394 | | (etr) ₈ -(C120) ₅ -P _{hCMVmin} -LFY-VP16-NLS-2A-RLuc-T _{SV40} | LFY-linker-VP16-NLS was amplified from pROF367 with oligos oROF427/oROF429. 2A-linker-RLuc was amplified from pROF202 with oligos oROF420/oROF392. | pROF021 digested with EcoRI/SpeI | Gibson cloning of backbone and the PCR |

| | | | | | |
|---------|---------|---|--|--|--|
| ↳ | pROF367 | P _{CaMV35S} -LFY-VP16-NLS-T _{nos} | LFY-VP16-NLS was amplified from pJA082 with oligos oROF404/oROF405 | pGEN016 ²⁹ digested with AgeI/EcoRI | Gibson assembly of backbone and PCR insert |
| ↳ | pJA082 | P _{SV40} -LFY-VP16-NLS-HAtag-T _{SV40} | LFY (At5g61850) was amplified from Arabidopsis cDNA with oligos oJA181/oJA163. VP16 was amplified from pKM018 ⁷ with oligos oJA060/oSLS466 | pMZ333 ²⁵ digested with NotI/XbaI | AQUA cloning |
| ↳ | pROF202 | 2A-linker-RLuc (Pos. B5) | 2A-linker-RLuc was generated with sequential PCRs. First PCR was amplified from pSW209 ³⁰ with oligos oROF205/oROF207, and this product was used as template with oligos oROF206/oROF207. | pUPD2 ³¹ | BsmBI restriction-ligation reaction (GB) |
| pROF402 | | P _{35S} enhancer(-953 to -51)-(C120) ₅ -P _{hCMVmin} -FLuc-T _{35S} | pROF339, pROF054, pROF375, GB0096 ²⁰ , GB0036 ²⁰ | pDGB 1alpha ²⁰ | BsaI restriction-ligation reaction (GB) |
| ↳ | pROF339 | P _{35S} enhancer(-953 to -51) (Pos. A1) | P _{35S} enhancer(-953 to -51) was amplified from GB0030 ²⁰ with oligos oROF377/oROF378 | pUPD2 ³¹ | BsmBI restriction-ligation reaction (GB) |
| ↳ | pROF054 | (C120) ₅ (Pos. A2) | (C120) ₅ was amplified from pGL4.32-C120-FLuc ²⁶ with oligos oROF073/oROF074 | pUPD2 ³¹ | BsmBI restriction-ligation reaction (GB) |
| ↳ | pROF375 | P _{hCMVmin} (Pos. A3-B2) | P _{hCMVmin} was amplified from pMZ836 ¹⁹ with oligos oROF083/oROF084 | pUPD2 ³¹ | BsmBI restriction-ligation reaction (GB) |
| pROF417 | | P _{CaMV35S} -LFY-VP16-NLS-2A-RLuc-T _{nos} | LFY-linker-VP16-NLS was amplified from pROF367 with oligos oROF404/oROF429. 2A-linker-RLuc was amplified from pROF202 with oligos oROF420/oROF474 | pGEN016 ²⁹ digested with AgeI/EcoRI | Gibson assembly of backbone and PCR insert |

| | | | | | |
|---------|---------|--|--|----------------------------|--|
| pROF441 | | $P_{AtU6-26}$ -gRNA(P_{AtAP1})-sgRNA | gRNA(P_{AtAP1}) was constructed using oligos oROF537/oROF538 at 1 μ M; 5 μ l of each were mixed and incubated for 30 min at RT. Then 1 μ l of the mixture was combined with pROF440 and pROF446. | pDGB 1alpha ²⁰ | BsaI restriction-ligation reaction (GB) |
| ↳ | pROF440 | $P_{AtU6-26}$ (Pos. A1-B2) | $P_{AtU6-26}$ was amplified from pEn-Chimera ³² with oligos oROF137/oROF545 | pUPD2 ³¹ | BsmBI restriction-ligation reaction (GB) |
| ↳ | pROF446 | sgRNA | sgRNA was amplified from pEN-Chimera ³² with oligos oROF546/oROF140 | pUPD2 ³¹ | BsmBI restriction-ligation reaction (GB) |
| pROF449 | | (etr) ₈ -(C120) ₅ - $P_{hCMVmin}$ -dCas9-TV-T _{35S} | pROF053, pROF054, pROF375, GB1079 ²¹ , GB2001 ²¹ , GB0036 ²⁰ | pDGB 1alpha ¹²⁰ | BsaI restriction-ligation reaction (GB) |
| ↳ | pROF053 | (etr) ₈ (Pos. A1) | (etr) ₈ was amplified from pKM081 ²⁷ with oROF071/oROF072 | pUPD2 ³¹ | BsmBI restriction-ligation reaction (GB) |
| ↳ | pROF054 | (C120) ₅ (Pos. A2) | (C120) ₅ was amplified from pGL4.32-C120-FLuc ²⁶ with oligos oROF073/oROF074 | pUPD2 ³¹ | BsmBI restriction-ligation reaction (GB) |
| ↳ | pROF375 | $P_{hCMVmin}$ (Pos. A3-B2) | $P_{hCMVmin}$ was amplified from pMZ836 ¹⁹ with oligos oROF083/oROF084 | pUPD2 ³¹ | BsmBI restriction-ligation reaction (GB) |
| pRSET | | PT7-driven bacterial expression vector (ThermoFisher) | | | |

2A, F2A self-cleaving peptide derived from the foot-and-mouth disease virus; BRD, B3 repression domain from *A. thaliana*; (C120)₅, 5 repeats of the DNA cognate sequence of EL222; dCas9, CRISPR associated protein 9 nuclease deficient; E, macrolide-responsive repressor protein; EFR, LRR receptor-like serine/threonine-protein kinase from *A. thaliana*; EL222, transcription factor from *Erythrobacter litoralis*; (etr)₈, 8 repeats of the DNA cognate sequence of E; FLuc, Firefly luciferase; GBP, GFP binding protein; GFP, green fluorescent protein; gRNA, part of the guide RNA containing the 20 bp target sequence; GUS, β -glucuronidase from *E. coli*; H2B, *A. thaliana* histone B2; HA-tag, human influenza hemagglutinin-derived epitope tag; KRAB, transcriptional repressor domain from human Krüppel Associated Box; LFY, LEAFY transcription factor from *A. thaliana*; NLS, nuclear localization signal from the simian virus 40 large T antigen; nptII, neomycin phosphotransferase; P_{35S} enhancer(-953 to -51), enhancer region of the *cauliflower mosaic virus* 35S promoter; $P_{AtU6-26}$, *A. thaliana* U6-26 RNA polymerase III promoter; P_{AtAP1} , *A. thaliana* APETALA1 promoter; $P_{AtUbi10}$, *A. thaliana* Ubiquitin-10 promoter; $P_{CaMV35S}$, *cauliflower mosaic virus* 35S promoter; $P_{hCMVmin}$, minimal human cytomegalovirus

immediate early promoter; PhyB(1–650), N-terminus of *A. thaliana* phytochrome B with amino acids 1–650; PIF6(1–100), N-terminus of *A. thaliana* phytochrome-interacting factor 6 with amino acids 1–100; P_{nos}, *Agrobacterium tumefaciens* nopaline synthase promoter; P_{SIDFR}, *Solanum lycopersicum* dihydroflavonol 4-reductase promoter; P_{SV40}, simian virus 40 early promoter; RLuc, Renilla luciferase; SF, stuffer DNA fragment; SRDX, EAR repression domain from *A. thaliana*; SEAP, human secreted alkaline phosphatase; sgRNA, single guide RNA from combined bacterial crRNA and tracrRNA without the target sequence; T_{35S}, *cauliflower mosaic virus* 35S terminator; T_{3A}, ribulose-1,5-bisphosphate carboxylase 3A subunit terminator; T_{nos}, *A. tumefaciens* nopaline synthase terminator; T_{OCS}, *A. tumefaciens* octopine synthase terminator; T_{SV40}, simian virus 40 early terminator; TV, activation domain composed by 6x TAL and 2x VP64 and NLS sequence; VP16, *Herpes simplex* virus-derived transactivation domain.

Supplementary Table 2. Oligonucleotides used in this work (lowercase correspond to annealing part and uppercase corresponds to overhangs)

| Oligonucleotide name | Sequence 5'->3' |
|----------------------|--|
| oBM0083 | CTGTGGTCTCAGGAGcttccaagtttaaaccgattg |
| oBM0079 | CCCGAAGACTCCATTaggctggatcgggtcccg |
| oBM0080 | TGTGAAGACCAAATGatgcttgatcttgaacttagac |
| oBM0081 | CCCGAAGACTCAAGCcttagattccggcttcgac |
| oBM0205 | TGTGAAGACCAAATGactagtatggaagatg |
| oBM0206 | CCCGAAGACTCAAGCcttcgaggttacacggcg |
| oBM0207 | TGTGAAGACCAAATGtcgcaatggcttcg |
| oBM0208 | CCCGAAGACTCAAGCgcatcgcctattgttca |
| oBM0209 | TGTGAAGACCAggaggacgagtcagtaataaac |
| oBM0210 | CCCGAAGACTCattctgttaatcagaaaaac |
| oJA060 | TCTTCTTCTCACCATACCAACTGGTCTCTCACcggtgaattcgatagtgctggtagtctgtag |
| oJA163 | CACTACCAGCACTACCAGCACTATCGAATTCCTAGTgaaacgcaagtcgctgc |
| oJA181 | TTTTATTTTCAAGTCCCGGATCGAATTGCGGGCGCGGCCGCCACCatggatcctgaaggtttcacg |
| oNBA145 | AAGAAGACTATACGGGTCTCAAAGGgaatggcggatgtgaacctggtgg |
| oNBA146 | AAGAAGACTACAGAGGTCTCAGATTctgtacagctcgtccatg |
| oNBA160 | CGGGTCTCTGCGGcttccaagtttaaaccgattgaat |
| oNBA176 | GGTCTCACAGAGAaggctggatcgggtcccgggtgc |
| oNBA289 | TAGGTCTCACACCatgaagctgtcctttcacttg |
| oNBA290 | TAGGTCTCACCTTcatagtatgatgcccga |

| | |
|---------|--|
| oROF023 | TACCGGTTGGCTAGGTAAGCTTGGTACCACCTGAACGACGCATATGatctaagctagccccacca |
| oROF024 | GTTATCTAGATCCGGTGGATCCAAGCTTCTCGAGCCCGGGAATTCgggaggtgtgggaggtttt |
| oROF027 | tacgggaggtattggacagg |
| oROF028 | TGATGCCGCTAGCtctagtgtctaagcttcatgg |
| oROF068 | CCAAAGAAGAAGAGGAAGGTGGGAGCTGGAGCTggggcagacgacaca |
| oROF069 | AGGTAAGCTTGGTACCACCTGAACGACGCATATGGGTAATTCTAAGACTCTTAGACTTTTTGGTGTTAATATGGAATGTccaagaagaaga ggaaggt |
| oROF071 | GCGCCGTCTCGCTCGGGAGgtttaacgattgaatataaccgac |
| oROF072 | GCGCCGTCTCGCTCGGTCAgctagcatccctaaatgtaac |
| oROF073 | GCGCCGTCTCGCTCGTGACgctagcctcgagtaggtagc |
| oROF074 | GCGCCGTCTCGCTCGGGGAaagcttcatggactaaaggct |
| oROF083 | GCGCCGTCTCGCTCGTCCC GCGCCGCcctatataagcagagctcgtt |
| oROF084 | GCGCCGTCTCGCTCGCATTACCGGTaggctggatcgggtcccgggtg |
| oROF091 | GCGCCGTCTCGCAagacgcggatcggacacg |
| oROF092 | GCGCCGTCTCGCTTgccgacaatccgctgat |
| oROF093 | GCGCCGTCTCGCTCGAAGCttagattccggcttcgacgg |
| oROF095 | GCGCCGTCTCGCTCGAatgcttgatcttgaacttagactt |
| oROF100 | GCGCCGTCTCGCTCGAatgacaacaatgcccccccaaa |
| oROF101 | GCGCCGTCTCGCTCGAAGcctacaccttctcttcttctt |
| oROF137 | GCGCCGTCTCGCTCGGGAGcttttttcttcttcttctggtcatac |
| oROF140 | GCGCCGTCTCGCTCAAGCGtaatgccaactttgtacaagaaag |
| oROF205 | GAATCAAATCCTGGACCCGCGCGCGGTGCAGGCGCTGGAGCCGGTGCCGGGGCAGGCGCTGGCGCTatgacttcgaaagtttatgatcca |

| | |
|---------|--|
| oROF206 | GCGCCGTCTCGCTCGTTCGGACCCGTGAAACAGCTGCTCAACTTCGATCTCCTCAAACCTGGCCGGCGACGTGgaatcaaatcctggaccgg |
| oROF207 | GCGCCGTCTCGCTCAAAGCTTAgaattctgttcatttttgagaac |
| oROF377 | GCGCCGTCTCGCTCGGGAGagcatcgtgaaaaagaagac |
| oROF378 | GCGCCGTCTCGCTCAGTCAatagtggttggtgcgtcatc |
| oROF392 | ACGCGTATTTAAATTAATTAAGCGATCGCACTAGTTTAttgttcattttgagaactcgct |
| oROF401 | CCACCTGACGTCGTCGACGATCGACCTGCAGtgtttaacatccaagatttgttttac |
| oROF403 | CTGACTCTAGAGGATCCCCGGGCGAGCTCGAATTCcattttgatccttttaagaaact |
| oROF404 | TTTGGAGAGAACACGGGGACTCTAGCGCTACCGGTgcgggccaccat |
| oROF405 | CCGGTGGATCCAAGCTTCTCGAGCCCGGGAATTCCTAcacctccgctttttctggg |
| oROF406 | CCGGTGGATCCAAGCTTCTCGAGCCCGGGAATTCCTACACCTTCCGCTTTTTCTTGGGgaaacgcaagtcgtcgcc |
| oROF415 | TCTGATTAACAGATGCAGATCTTAATGTCGCGAatggtgagcaagggc |
| oROF417 | TGTTTGAACGATCTGCTTGACAAGCGCGATCGCTCACACCTTCCGCTTTTTCTTGGGgtaattaactgtacagctcg |
| oROF420 | cccgtgaaacagctg |
| oROF422 | agaactgcctgcgtgagatt |
| oROF423 | ttttccgtcatcgtctttcc |
| oROF424 | gaggcgaactgtgtgtgaga |
| oROF425 | gtgttcgtctctgtcccagt |
| oROF427 | ACCGATCCAGCCTCCGCGGCCCCGGTACCGAATTCgcgggccaccat |
| oROF429 | TTGAGCAGCTGTTTCACGGGcacctccgctttttctggg |
| oROF436 | GAAGACACCGGGACCGATCCAGCCTAATGACTAGTatggtgagcaagggcg |
| oROF442 | TCGATCGACTCTAGCTAGAGAAGCCCTGCAGGctagtaattaagaactcgtaaacctcg |
| oROF474 | GAAGACACCGGGACCGATCCAGCCTAATGACTAGTatgtctttctccgtga |

| | |
|---------|--|
| oROF514 | gtgaaaactgttgagagaagcaa |
| oROF515 | tcaactggatacccttgcga |
| oROF518 | ggtggtcgataaagatgttctga |
| oROF519 | aagcctctgactgatggagc |
| oROF537 | ATTGTATATCTCGTACTAATGTC |
| oROF538 | AAACGACATTAGTACGAGATATA |
| oROF545 | GCGCCGTCTCGCTCAaatcactactcgactctag |
| oROF546 | GCGCCGTCTCGCTCGgttttagagctagaaatagcaagt |
| oSLS466 | CTTGGGCTGCAGGTCGACTCTAGACTAAGCGTAATCTGGAACATCGTATGGGTacaccttccgcttttcttgggcc |

Supplementary Table 3. Estimated model parameters and confidence intervals on linear scale. Estimated parameters $\hat{\theta}$ were obtained by maximum likelihood estimation and their point-wise 95 % confidence intervals σ^- and σ^+ were obtained with the profile likelihood method. Fixed variables have no confidence intervals.

| Parameter | $\hat{\theta} (\hat{\theta} - \sigma^-, \hat{\theta} + \sigma^+)$ |
|---|---|
| <i>init_{FLuc}</i> | 5.35 (2.49, 8.26) •10 ⁻⁰³ |
| <i>b_{transcription}</i> | 0.83 (0.20, 15.8) •10 ⁻⁰¹ |
| <i>k_{transcript}</i> | 1.26 (0.86, 1.91) •10 ⁺⁰¹ |
| <i>k_{transl,FLuc}</i> | 1.46 (1.14, 1.95) •10 ⁻⁰³ |
| <i>k_{deg,FLuc}</i> | 1.32 (1.06, 1.68) •10 ⁻⁰¹ |
| <i>k_{deg,FLucmRNA}</i> | 0.81 (0.55, 1.22) •10 ⁺⁰⁰ |
| <i>k_{off,LOV}</i> | 5.10 (0.92, 6.30) •10 ⁻⁰¹ |
| <i>k_{on,LOV}</i> | 1.88 (0.60, 2.37) •10 ⁻⁰¹ |
| <i>k_{off,PhyBfr,dark}</i> | 1.24 (1.14, 1.35) •10 ⁻⁰¹ |
| <i>k_{off,PhyBr,red}</i> | 3.57 (2.97, 4.35) •10 ⁻⁰¹ |
| <i>scale_{FLuc,Exp1,Rep1}</i> | 8.27 (7.93, 8.63) •10 ⁺⁰⁰ |
| <i>scale_{FLuc,Exp1,Rep2}</i> | 6.75 (6.47, 7.04) •10 ⁺⁰⁰ |
| <i>scale_{FLuc,Exp1,Rep3}</i> | 8.10 (7.77, 8.45) •10 ⁺⁰⁰ |
| <i>scale_{FLuc,Exp1,Rep4}</i> | 4.01 (3.84, 4.18) •10 ⁺⁰¹ |
| <i>scale_{FLuc,Exp4,Rep1}</i> | 1.68 (1.62, 1.74) •10 ⁺⁰¹ |
| <i>scale_{FLuc,Exp4,Rep2}</i> | 8.79 (8.47, 9.11) •10 ⁺⁰⁰ |
| <i>scale_{FLuc,Exp5,blue}</i> | 1.25 (1.19, 1.32) •10 ⁺⁰¹ |
| <i>scale_{FLuc,Exp5,red}</i> | 4.02 (3.84, 4.21) •10 ⁺⁰¹ |
| <i>scale_{FLucmRNA,Exp3,Rep2}</i> | 1.45 (1.09, 2.01) •10 ⁺⁰⁰ |
| <i>sd_{FLuc,Exp1}</i> | 3.17 (2.78, 3.65) •10 ⁻⁰³ |
| <i>sd_{FLuc,Exp4}</i> | 6.34 (5.52, 7.38) •10 ⁻⁰³ |
| <i>sd_{FLuc,Exp5}</i> | 4.63 (3.96, 5.51) •10 ⁻⁰³ |
| <i>sd_{FLuc,Exp2}</i> | 4.19 (3.56, 5.00) •10 ⁻⁰³ |
| <i>sd_{FLucmRNA,Exp3}</i> | 3.58 (2.87, 4.62) •10 ⁺⁰⁰ |
| <i>k_{inh,LOV}</i> | 2.50•10 ⁺⁰¹ |
| <i>k_{off,PhyBr,farred}</i> | 1.00•10 ⁺⁰³ |
| <i>Γ_{PhyBfr,red}</i> | 7.28•10 ⁻⁰¹ |
| <i>Γ_{PhyBfr,farred}</i> | 2.00•10 ⁻⁰³ |

Supplementary References

1. De Caluwé, J. *et al.* A Compact Model for the Complex Plant Circadian Clock. *Front. Plant Sci.* **7**, 74–74 (2016).
2. Pokhilko, A. *et al.* The clock gene circuit in Arabidopsis includes a repressilator with additional feedback loops. *Mol. Syst. Biol.* **8**, 574 (2012).
3. Locke, J. C. W., Millar, A. J. & Turner, M. S. Modelling genetic networks with noisy and varied experimental data: the circadian clock in Arabidopsis thaliana. *J. Theor. Biol.* **234**, 383–393 (2005).
4. Raue, A. *et al.* Lessons Learned from Quantitative Dynamical Modeling in Systems Biology. *PLoS ONE* **8**, e74335 (2013).
5. Beyer, H. M. *et al.* Synthetic Biology Makes Polymer Materials Count. *Adv. Mater.* **30**, 1800472 (2018).
6. Raue, A. *et al.* Structural and practical identifiability analysis of partially observed dynamical models by exploiting the profile likelihood. *Bioinformatics* **25**, 1923–1929 (2009).
7. Müller, K. *et al.* A red/far-red light-responsive bi-stable toggle switch to control gene expression in mammalian cells. *Nucleic Acids Res.* **41**, e77–e77 (2013).
8. Kelly, J. M. & Lagarias, J. C. Photochemistry of 124-kilodalton Avena phytochrome under constant illumination in vitro. *Biochemistry* **24**, 6003–6010 (1985).
9. Legris, M. *et al.* Phytochrome B integrates light and temperature signals in Arabidopsis. *Science* **354**, 897 (2016).
10. Raue, A. *et al.* Data2Dynamics: a modeling environment tailored to parameter estimation in dynamical systems. *Bioinformatics* **31**, 3558–3560 (2015).
11. Hindmarsh, A. C. *et al.* SUNDIALS: Suite of nonlinear and differential/algebraic equation solvers. *ACM Trans. Math. Softw.* **31**, 363–396 (2005).
12. Coleman, T. & Li, Y. An Interior Trust Region Approach for Nonlinear Minimization Subject to Bounds. *SIAM J. Optim.* **6**, 418–445 (1996).
13. Kreutz, C., Raue, A. & Timmer, J. Likelihood based observability analysis and confidence intervals for predictions of dynamic models. *BMC Syst. Biol.* **6**, 120 (2012).
14. Sellaro, R. *et al.* Cryptochrome as a Sensor of the Blue/Green Ratio of Natural Radiation in Arabidopsis. *Plant Physiol.* **154**, 401 (2010).
15. Casal, J. J. Photoreceptor Signaling Networks in Plant Responses to Shade. *Annu. Rev. Plant Biol.* **64**, 403–427 (2013).

16. Feike, D. *et al.* Characterizing standard genetic parts and establishing common principles for engineering legume and cereal roots. *Plant Biotechnol. J.* **17**, 2234–2245 (2019).
17. Weber, E., Engler, C., Gruetzner, R., Werner, S. & Marillonnet, S. A Modular Cloning System for Standardized Assembly of Multigene Constructs. *PLoS ONE* **6**, e16765 (2011).
18. Calderon-Villalobos, L. I. A. *et al.* LucTrap Vectors Are Tools to Generate Luciferase Fusions for the Quantification of Transcript and Protein Abundance in Vivo. *Plant Physiol.* **141**, 3 (2006).
19. Müller, K. *et al.* A red light-controlled synthetic gene expression switch for plant systems. *Mol. Biosyst.* **10**, 1679–1688 (2014).
20. Sarrion-Perdigones, A. *et al.* GoldenBraid 2.0: A Comprehensive DNA Assembly Framework for Plant Synthetic Biology. *Plant Physiol.* **162**, 1618 (2013).
21. Selma, S. *et al.* Strong gene activation in plants with genome-wide specificity using a new orthogonal CRISPR/Cas9-based programmable transcriptional activator. *Plant Biotechnol. J.* **17**, 1703–1705 (2019).
22. Binder, A. *et al.* A Modular Plasmid Assembly Kit for Multigene Expression, Gene Silencing and Silencing Rescue in Plants. *PLoS ONE* **9**, e88218 (2014).
23. Schornack, S. *et al.* Protein mislocalization in plant cells using a GFP-binding chromobody. *Plant J.* **60**, 744–754 (2009).
24. Schwessinger, B. *et al.* Phosphorylation-Dependent Differential Regulation of Plant Growth, Cell Death, and Innate Immunity by the Regulatory Receptor-Like Kinase BAK1. *PLoS Genet.* **7**, e1002046 (2011).
25. Baaske, J. *et al.* Dual-controlled optogenetic system for the rapid down-regulation of protein levels in mammalian cells. *Sci. Rep.* **8**, 15024 (2018).
26. Motta-Mena, L. B. *et al.* An optogenetic gene expression system with rapid activation and deactivation kinetics. *Nat. Chem. Biol.* **10**, 196–202 (2014).
27. Müller, K. *et al.* Multi-chromatic control of mammalian gene expression and signaling. *Nucleic Acids Res.* **41**, e124 (2013).
28. Bleckmann, A. Untersuchungen zur Stammzellregulation im Sprossapikalmeristem von *Arabidopsis thaliana*. (PhD Thesis, Heinrich-Heine-Universität Düsseldorf, 2010).
29. Samodelov, S. L. *et al.* StrigoQuant: A genetically encoded biosensor for quantifying strigolactone activity and specificity. *Sci. Adv.* **2**, e1601266 (2016).

30. Wend, S. *et al.* A quantitative ratiometric sensor for time-resolved analysis of auxin dynamics. *Sci. Rep.* **3**, 2052 (2013).
31. Vazquez-Vilar, M. *et al.* GB3.0: a platform for plant bio-design that connects functional DNA elements with associated biological data. *Nucleic Acids Res.* **45**, 2196–2209 (2017).
32. Fauser, F., Schiml, S. & Puchta, H. Both CRISPR/Cas-based nucleases and nickases can be used efficiently for genome engineering in *Arabidopsis thaliana*. *Plant J.* **79**, 348–359 (2014).